LBL-17643
Preprint c.2

Lawrence Berkeley Laboratory

UNIVERSITY OF CALIFORNIA

RECEIVED
LAWRENCE
BERKELEY LABORATORY

DEC 19 1984

LIBRARY AND
DOCUMENTS SECTION

Submitted to Nuclear Instruments and Methods

AN ELECTRON-BEAM-GENERATED-PLASMA ION SOURCE FOR ON-LINE ISOTOPE SEPARATION

J.M. Nitschke

September 1984

TWO-WEEK LOAN COPY
This is a Library Circulating Copy which may be borrowed for two weeks.

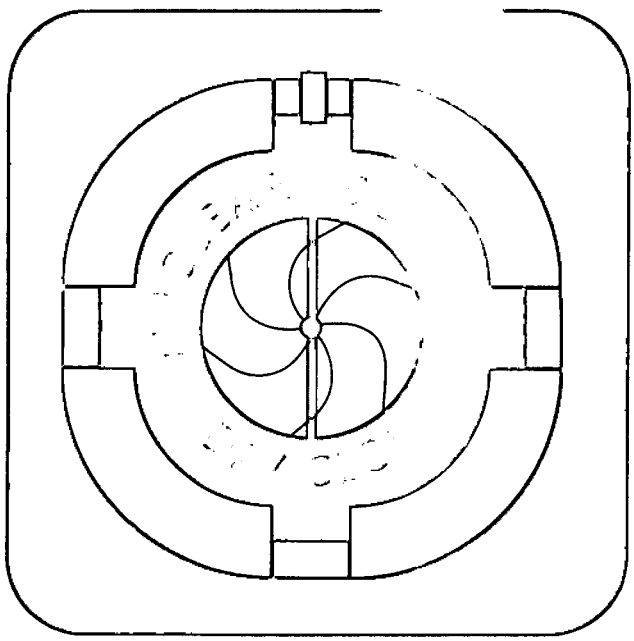

Prepared for the U.S. Department of Energy under Contract DE-AC03-76SF00098

LBL-17643 c.2

DISCLAIMER

This document was prepared as an account of work sponsored by the United States Government. While this document is believed to contain correct information, neither the United States Government nor any agency thereof, nor the Regents of the University of California, nor any of their employees, makes any warranty, express or implied, or assumes any legal responsibility for the accuracy, completeness, or usefulness of any information, apparatus, product, or process disclosed, or represents that its use would not infringe privately owned rights. Reference herein to any specific commercial product, process, or service by its trade name, trademark, manufacturer, or otherwise, does not necessarily constitute or imply its endorsement, recommendation, or favoring by the United States Government or any agency thereof, or the Regents of the University of California. The views and opinions of authors expressed herein do not necessarily state or reflect those of the United States Government or any agency thereof or the Regents of the University of California.

LBL-17643

An Electron-Beam-Generated-Plasma Ion Source for On-line Isotope Separation*

J. M. Nitschke

Nuclear Science Division
Lawrence Berkeley Laboratory
University of California
Berkeley, California 94720

*This work was supported by the Director, Office of Energy Research, Division of Nuclear Physics of the Office of High Energy and Nuclear Physics of the U.S. Department of Energy under Contract DE-AC03-76SF00098.

LBL-17643

An Electron-Beam-Generated-Plasma Ion Source for On-line Isotope Separation*

J. M. Nitschke

Nuclear Science Division
Lawrence Berkeley Laboratory
University of California
Berkeley, California 94720

Abstract

A novel ion source based on an electron-beam-generated plasma is described. It features high efficiency and high temperature operation (~3000 K). It does not incorporate magnetic fields and delivers beams of high quality suitable for mass spectrometry. No support gas per se is required. The plasma theoretical principle of the source is investigated and ionization-efficiencies, delay times, charge carrier densities, pressure limits, current densities etc. are calculated. These calculations are compared with experiments and computer simulations.

*This work was supported by the Director, Office of Energy Research, Division of Nuclear Physics of the Office of High Energy and Nuclear Physics of the U.S. Department of Energy under Contract DE-AC03-76SF00098.

Table of Contents

1. Introduction

2. The Operating Principle of the Electron-Beam-Generated-Plasma Ion Source

3. Quantitative Considerations

   3.1 Ionization

   3.2 Plasma Parameters

   3.3 Space Charge Compensation

4. Experimental Results

5. Mechanical and Electrical Aspects of the Source Design

6. Computer Simulation

7. Conclusion and Acknowledgments

8. References

1. Introduction

The heart of an on-line isotope separator is the ion source. Its properties determine the scientific usefulness of the separator for the study of exotic isotopes far from stability. The most important parameters of the source are: (1) high efficiency, (2) short delay times for radioactive species with short half-lives, and (3) high temperature operation to achieve short release times and to prevent the condensation of elements with low vapour pressure. Other requirements are (4) low energy spread of the extracted ion beam, (5) chemical selectivity, (6) versatility to adapt to different target configurations and to different reaction mechanisms, (7) long life time, and (8) electrical and mechanical stability.

The ideal ion source that fulfills all of these requirements does not exist. The reasons for this are theoretical as well as practical. The physics of ion sources is quite complex due to the large number and types of processes that have to be considered: ionization, recombination, charge exchange, interactions with electrodes on different potentials, adsorption and desorption, high temperature effects, chemical reactions, dissociation, transport phenomena, diffusion, collective effects, and oscillations to name only a few. Further complications arise from the presence of magnetic fields and from strong electric gradients at the extraction opening. Very few measurements of the plasma conditions in ion sources exist and some of the most detailed experiments and their interpretation were carried out many years ago [1]. Associated with the complex physics are great difficulties in treating ion sources mathematically. The usual "prescriptions" of plasma physics can rarely be applied because of the small dimensions of the discharge chamber. One consequence of this is that there is also no computer model or simulation available.

Practical reasons for the nonexistence of the ideal ion source are related to the properties of the construction materials. In on-line isotope separation many elements of interest have low vapour pressure and the sources have to be operated at the highest possible temperatures to prevent condensation and to achieve short release times from the catcher or target material. For temperatures above 2500 C only carbon, molybdenum, tantalum and tungsten can be used for ion source parts. Insulators are even more restricted in their highest operating temperature; and materials like boron nitrite, zirconia, thoria, and beryllia become conductive and mechanically unstable at temperatures at or above 2000 C. Some insulators decompose in contact with graphite or metals increasing the residual gas pressure inside the ion source. For ion sources of the type described in this paper this is highly undesirable, since they operate with little or no support gas. Several of these practical problems are discussed in [2], a recent review of the ion-source development for on-line separators is given in [3] and of plasma ion sources in general in [4].

2. The Operating Principle of the New Ion Source

Symbols and units:

A_{ex} = area of the extraction opening (m^2).

A_S = inner surface of the ion source (m^2).

D = distance between the virtual cathode and the anode (m).

E,eU = energy (eV)

e/m = charge to mass ratio of the electron ($=1.759 \times 10^{11}$ C/kg).

ϵ_o = permittivity of the vacuum ($=8.854 \times 10^{-12}$ F/m).

η = ionization efficiency (%).

I = electrical current (A).

J = current density (A/m) or (A/m^2).

J_i^* = ion current density near the extraction opening (A/m^2).

k = Boltzmann's constant ($=1.381 \times 10^{-23}$ J/K).

κ = ratio of the electron density at the anode grid to the electron density near the axis of the source.

ℓ = ionization length (m).

λ = free mean path (m).

λ_D = Debeye length (m).

m = mass (kg).

M = mass value (AMU).

n = number density (m^{-3}).

n_w = number of collisions with the ion source wall.

n* = standard neutral density at 273 K and 1 Torr ($=3.53 \times 10^{22}$ m^{-3}).

N = power (W).

N_D = number of electrons in a Debeye sphere .

ν = average number of oscillations of an electron in the ionization region of the source.

p^* = critical ion source pressure (Torr) (see text).

ϕ = space charge potential (V).

$\Delta\phi$ = potential difference between the anode and the plasma (V).

q = differential ionization (m^{-1}).

Q = cross section (m^2).

r = radius of the ion source anode cylinder (m).

R = molecular flow conductance ratio.

ρ = space charge density (As/m^3).

T = temperature (K).

$\bar{\tau}$ = average time an atom spends inside the ionization volume (s).

u = one dimensional ion velocity (m/s).

$\check{u}$ = minimum ion velocity to overcome the potential difference $\Delta\phi$ (m/s) (see text).

v = velocity (m/s).

V_o = cathode potential (V).

V_i = ionization threshold of the residual gas (V).

x = coordinate for the one dimensional diode configuration.

X = degree of ionization (%).

$\bar{z}$ = average charge

Subscripts:

a = atom

A = Anode

e = electron

ex = extraction

i = ion

p = plasma

The ion source to be described has been used extensively in on-line and off-line experiments at the OASIS facility [5] at the Berkeley SuperHilac. Energetic recoils from heavy ion reactions are ejected from a target (1-3 mg/cm^2) and are admitted to the source through a thin tungsten window (~ 1-2 mg/cm^2) or a bundle of capillary tubes. The recoils are imbedded in one of the inner walls of the ion source which is kept at a temperature of $\gtrsim$ 2500 K. At this elevated temperature the recoils diffuse rapidly out of the wall material and fill the ion source volume as a radioactive gas. This gas together with any residual, non radioactive gas is ionized by electron bombardment, and the ions are extracted, accelerated and analyzed magnetically.

The operating principle of the ion source can best be understood by referring to figs. 1a and b which show an idealized version of the actual device. The anode of the source consists of two circular end pieces mechanically and electrically connected by a cylindrical grid. One end wall acts as a window that admits the radioactive species and the other has a central opening for the extraction of the ion beam. The grid is surrounded at close distance by a coaxial cathode. The cathode is indirectly heated by electron bombardment and kept at a negative potential V_0 (typically ~100 V) with respect to the anode. The whole ion source is operated at a high potential V_{ex} (typically 10-30 KV) with respect to an extraction electrode located in front of the perforated anode endplate. The function of this electrode is to extract, accelerate and shape the ion beam.

The operation of the source can be analyzed in two steps: a start up phase and a steady state phase. During the initial part of the start up phase it is assumed that the ion source operates in perfect vacuum. Electrons from the inside surface of the cathode cylinder are attracted towards the anode grid by the potential V_0; they traverse the grid and enter the inner

volume of the anode cylinder. At low current densities negligible space charge forces exist and the electrons traverse the anode cylinder, get reflected at the cathode and return to the inner volume of the anode. At higher current densities the electrons are influenced by the space charge forces created by other electrons; in particular near the axis. If I is the electron current per unit length of the anode cylinder with radius r, then the current density is:

$$J = \frac{I}{2\pi r} \quad . \tag{1}$$

The potential ϕ and the space charge density ρ are then related by Poisson's equation in cylindrical coordinates:

$$\frac{1}{r}\frac{\partial}{\partial r}\left(r\frac{\partial\phi}{\partial r}\right) = -\frac{\rho}{\varepsilon_0} = -\frac{I}{\varepsilon_0 2\pi r v} \quad ; \tag{2}$$

where ε_0 is the permittivity of the vacuum and v the velocity of the electrons:

$$v(r) = \sqrt{\frac{2e}{m}(V_0 + \phi\,(r))} \tag{3}$$

e/m is the charge to mass ratio of the electron.

With $$A \equiv -\frac{I}{2\pi\varepsilon_0\sqrt{2e/m}} \tag{4}$$

and $$U(r) \equiv V_0 + \phi(r) \tag{5}$$

eq. (2) becomes:

$$\frac{\partial}{\partial r}\left(r\,\frac{\partial U}{\partial r}\right) = AU^{-1/2} \quad . \tag{6}$$

Expression (6) is a nonlinear equation which does not lend itself to a simple, analytical solution. A solution of Poisson's equation in cylindrical coordinates may, however, not be necessary as can be shown by considering the space charge effects in the planar configuration (fig. 2).

Electrons from a flat cathode at a negative potential V_o are accelerated towards an anode grid at ground potential. After traversing the grid their motion is determined by the one dimensional Poisson equation:

$$\frac{\partial^2 \phi}{\partial x^2} = -\frac{\rho}{\varepsilon_o} = -\frac{J}{\varepsilon_o v} \quad . \tag{7}$$

The symbols have the same meanings as in the previous equations except that in this case J is the current density per unit area, and $\phi(r)$ becomes $\phi(x)$. Again we set $v = \sqrt{\frac{2e}{m}\left(V_o + \phi(r)\right)}$, $A \equiv -\frac{J}{\varepsilon\sqrt{2e/m}}$ and $U(x) \equiv V_o + \phi(x)$ Eq. (7) then becomes:

$$\frac{d^2U}{dx^2} = AU^{-1/2} \quad . \tag{8}$$

Integrating eq. (8) under the conditions $U(o) = V_o$ and $\frac{dU}{dx}(\phi = -V_o) = 0$ gives:

$$U(x) = \left(-\frac{3}{2}\left(\frac{m}{2e\varepsilon_o^2}\right)^{1/4}\sqrt{|J|}\;x + V_o^{3/4}\right)^{4/3} \quad . \tag{9}$$

In SI units:*

---

*SI units are used throughout this paper unless noted otherwise.

$$U(x) = (-654.6\sqrt{|J|}\, x + V_o^{3/4})^{4/3} \quad (V) \tag{9a}$$

At a sufficiently large distance D from the anode the (negative) space charge potential ϕ will become equal to the initial accelerating potential V_o of the cathode and bring the electrons to a halt. They will then return to the anode grid and be reflected by the cathode. The distance D is sometimes referred to as the location of the "virtual cathode." D can be obtained from eq. (9) under the condition $U(x = D) = 0$.

$$D = \left| \frac{4}{9}\, \epsilon_o \sqrt{\frac{2e}{m}}\, \frac{V_o^{3/2}}{|J|} \right|^{1/2} \quad ; \tag{10}$$

In fig. 3 eq. (9a) has been plotted for current densities of $J = 10^3$, 4×10^3, and 1.6×10^4 A/m^2 for a fixed cathode potential $V_o = 100$ V. A typical current density for the OASIS ion source is 4×10^3 A/m^2 which would in the <u>planar</u> case result in a virtual cathode located .76 mm from the anode. In the cylindrical case (cylinder radius ~4 mm) one would expect an even shorter distance due to the influence of the other electrons from all directions. The initial picture is, therefore, that in the absence of ions the electrons form a <u>space charge well</u> that fills a large portion of the anode volume. The depth of the well is equal to the cathode potential.

In the next step the electrons interact with the residual gas and ions are formed in the region between the anode and the virtual cathode. The ions are accelerated towards the axis of the source and become trapped in the space charge well.* Their initial energies E_i are $V_i \leq E_i \leq V_o$; where V_i is the ionization threshold. Since <u>all</u> ions gradually accumulate in the

---

*A device using a small central filament was first used by Kingdon [6].

negative well, the potential ϕ_p which results from the combined positive ion- and negative electron-space charge becomes less and less negative.* This allows the electrons to penetrate further into the anode volume which in turn increases the ion production rate and the compensation of the electron space charge. As ϕ_p rises, ions with energies larger than $e\phi_p$ are able to leave the well and are neutralized at the anode or the cathode. The remaining low energy ions are particularly effective in compensating the electron space charge and the space charge compensation process continues until in the final phase steady state conditions are reached. This phase of the ion source operation is characterized by a slightly negative space charge potential inside the anode volume in which the ions have essentially thermal energies. This is important in order to achieve a high mass-resolution of the separator. The ion energy distribution is maxwellian and the space charge potential adjusts itself such that the ion production is balanced by ion losses to the walls or due to extraction;** i.e. if the ion production becomes too high, the space charge potential rises, and positive ions "spill over the edge" of the space charge well and are collected by the anode or cathode. This happens at high residual gas pressures. The hole in one of the circular anode end plates and the negative extraction voltage create a "snout" in the space charge "bucket" through which ions leave the ionization volume (fig.1d). It is important to notice that in the low pressure operation the

---

*It should be pointed out that ions are very effective in compensating the electron space charge since their velocity v_i is about 2×10^{-3} of the electron velocity v_e for the same potential. After only thermal ions remain, the ion velocity drops to about 1×10^{-4} v_e.

**Note that an interesting "ion cooling" process is taking place, where the most energetic ions are eliminated and the lower energy ones remain in the space charge well.

extracted ion current is equal to the total ion production rate in the entire anode volume. This is quite different from the usual condition in a plasma ion source, and is the principal reason for the high efficiency of the electron-beam-generated-plasma (EBGP) source. In the common plasma source the ion current through the extraction opening is only a small fraction of the ion current to the wall through the plasma sheath. This fraction is determined by the ratio of the effective area of the extraction opening to the total surface area of the discharge chamber.

The condition for efficient ion extraction is that the plasma potential "connects" with the potential surface created by the extraction voltage. If either the extraction gradient or the plasma potential are too low the extraction opening is effectively closed off for low energy ions.

Since the electron space charge in the source is nearly completely compensated, the energy of the primary electrons inside the anode volume is $eU_e = e(V_0 + \Delta\phi)$, where $\Delta\phi$ is on the order of -1 V. V_0 is chosen such that it coincides with the maximum of the ionization cross section and this optimal electron energy is thus maintained over the entire ionization region. Low energy "plasma electrons" that are created in the ionization process leave the plasma during a single path and "free fall" to the anode. Their contribution to the negative space charge potential is negligible because of their relatively high energies (~10 eV) and their low abundance; (the ratio of the primary electron current to the plasma electron current is typically > 10^6:1).*

---

*The large ratio of primary to "plasma" (or secondary) electrons is also the reason why the latter do not contribute significantly to the ionization process.

3. Quantitative Considerations

3.1 Ionization

It was pointed out in the previous chapter that it is difficult to obtain direct measurements of most of the crucial parameters of the ion-source i.e. electron- and ion-temperatures, neutral- and ion densities, plasma potentials etc. It is, however, possible to obtain a consistent set of values for many parameters through a combination of indirect measurements* and calculations. Figure 4 shows a mass spectrum of the extracted ion beam from 1 to 300 AMU for a "cold spot" temperature of about 2400 K with small, calibrated leaks of $^{natl.}Xe$, $^{natl.}Kr$ and $^{natl.}Ar$ attached to the source. The spectrum is dominated by peaks of Ta, TaO, and CO. Based on the operating principle outlined in the previous chapter it is possible to calculate the magnitude of the ^{181}Ta current I_i from the following equation:

$$I_i = \nu I_e \ell q_i \frac{n}{n^*} \text{ (A)} \quad ; \tag{11}$$

n is the number density of Ta atoms at a "cold spot" temperature of 2400 K** ($n = 6.4 \times 10^{14}\ m^{-3}$) which can be calculated from the known vapour pressure of Ta at this temperature (2×10^{-7} Torr). The differential ionization q_i of Ta by 100 eV electrons is on the order of $1.5 \times 10^3\ m^{-1}$ [7], [8]. The electron current I_e is .53 A and the ionization length ℓ

---

*Several measurements were made with the ion source attached to the isotope separator magnet.

**This is the temperature of the Ta cathode necessary to achieve an electron current density of $6.3 \times 10^3\ A/m^2$.

is taken to be equal to the diameter of the source $(8.1 \times 10^{-3}\text{m})$. n^* is the standard density at 273 K and 1 Torr: $3.53 \times 10^{22}\ \text{m}^{-3}$; and ν is the average number of oscillations an electron makes through the anode volume before being captured by the anode grid. For an anode grid transmission of 53% $\nu = 1.4$. For ^{181}Ta eq. (11) yields a total ion current of 1.6×10^{-7} A. The measured, extracted ion current is 2×10^{-7} A which is in excellent agreement with the calculation considering the uncertainties in the values of the input parameters, particularly n. It also proves that--as pointed out in the previous chapter—the <u>total</u> ion current produced in the <u>entire</u> ionization volume is being extracted.

The above calculation for the ionization of Ta under constant vapour pressure conditions can in general not be applied to obtain the ionization efficiency of radioactive species. Their degree of ionization X(%) can, however, be obtained in the following way: The number of wall collisions n_W a neutral atom makes before it leaves the ion source is equal to the inner surface area of the source A_s divided by the area of the exit hole A_{ex}: $n_W = A_s/A_{ex}$, and the average distance it travels between wall collisions is taken to be the diameter 2r of the source. Its average thermal velocity is $\bar{v} = 1.46 \times 10^2 \sqrt{T/M}$ (m/s) where the temperature T is measured in degrees K and M is the mass value of the atom.

The average time $\bar{\tau}$ an atom spends inside the ionization volume is therefore

$$\bar{\tau} = 1.36 \times 10^{-2} r \frac{A_s}{A_{ex}} \sqrt{M/T} \quad (\text{s}) \quad . \tag{12}$$

In the case of the OASIS ion source this time is on the order of 1 ms for

medium heavy ions (A = 100). The degree of ionization X(%) then is related to the time $\bar{\tau}$ which the atom spends in the beam of the ionizing electrons via the following equation [9]:

$$\bar{\tau} = 28.3 \frac{X}{\nu J_e q_i} \left(1 + \frac{1}{\sqrt{1 - X/100}}\right) \text{ (s)} \quad . \tag{13}$$

In fig. 5 $q_i \bar{\tau}$ is plotted as a function of X for an electron beam density of 3.9×10^3 A/m^2. In cases where the differential ionization q_i is known and $\bar{\tau}$ is calculated from eq. (12) the degree of ionization for any atom can be obtained from the graph (fig. 5). It has been found that the experimentally observed degrees of ionization amount to about 60 of the calculated values. Figure 5 also shows that the ionization of heavy atoms is favoured considerably because of their longer delay times and their larger cross sections.

Two important quantities for the understanding of the functioning of the ion source are the mean free path of the electrons (λ_e) and the mean free path for ion-atom charge exchange collisions λ_{ia}. These two quantities are related to their respective cross section Q via $\lambda = (n_n Q)^{-1}$ where n_n is the density of the neutral atoms. A typical value for n_n is 4×10^{15} m^{-3} (10^{-6} Torr) for a "cold spot" temperature of about 2400 K. Total elastic cross sections for 20 to 100 eV electrons in medium-mass gases are on the order of 3×10^{-19} m^2 [10] which results in a free mean path for the electrons of $\lambda_e \approx 830$ m. The electrons will therefore traverse the ionization volume several times by being reflected at the cathode, before they are eventually intercepted by the anode grid.

The second phenomenon is the charge exchange between ions and atoms. An estimate of the magnitude of this effect is important because in practically all

cases the charges of the radioactive ions of interest can only be lost to neutral atoms of the "background gas" which are many orders of magnitude more abundant. The ion-atom charge exchange cross section Q_{ia} has for example been measured for $Cs^+ + Cs \rightarrow Cs + Cs^+$ over an energy range of .16 to 6.25 eV [11]; it is on the order of 10^{-18} m^2. This results in a free mean path for ion-atom charge exchange collisions of 250 m. The average (thermal) velocity of medium mass ions at 2400 K is ~800 m/s and the average time between collisions therefore 300 ms. This time is long compared to the average time an ion (or atom) spends inside the anode volume of the OASIS ion souce which is on the order of 1 ms as shown above. At a source pressure of 10^{-6} Torr losses due to ion-atom charge exchange collisions are therefore negligible. A "support gas" would, however, be highly detrimental to the operation of the source if its pressure reaches the order of 10^{-4} to 10^{-5} Torr (c.f. Section 4).

3.2 Plasma Parameters

According to Langmuir a plasma is a partially ionized gas in which the charged particles distribute themselves so as to achieve local, electric neutrality. The region over which such neutrality occurs is characterized by λ_D the so called Debeye length. This length has to be small compared to the macroscopic dimensions of the plasma. Two particles are effectively shielded from interacting with each other when their separation exceeds a distance on the order of λ_D. For this to occur the number of electrons N_D in a sphere of radius λ_D (called the Debeye sphere) has to be large. Another important characteristic of a plasma is its quasi neutrality with the ion density $\sum_j \bar{z}_j n_{ij}$ approximately equal to the electron density density n_e; where $\bar{z}_j$ is the average ionic charge of the ion with index j.

Expressions for λ_D and N_D are

$$\lambda_D = 7.43 \times 10^3 \sqrt{T_e/n_e} \quad (m)^{*} \tag{14}$$

and $$N_D = 1.72 \times 10^{12} \sqrt{T_e^3/n_e} \quad , \tag{15}$$

where the electron temperature T_e is measured in eV. Taking the "worst case" values for the OASIS ion source i.e. the electron density near the anode grid multiplied by the reflection factor (see chapter 3.1), and the primary electron energy-equivalent as the electron "temperature" results in $\lambda_D \leq 1$ mm and $N_D \leq 2.3 \times 10^7$. The $\leq$ sign indicates that both values become

*The concept of temperature and Debeye length has been extended here to monoenergetic, unidirectional electrons.

smaller towards the axis of the source. Their absolute values are such that the basic concept of the source as being based on an electron beam generated plasma (EBGP) is justified. The electrical neutrality $n_e = \sum_j z_j n_{ij}$ of the plasma is assured by the space charge compensation mechanism described in section 2.

A theoretical treatment of a beam generated plasma was attempted in [12]. This theory is, however, difficult to apply to the EBGP ion source because it considers only the case when the ratio of the beam generated electron density to the secondary plasma electron density is small, while in the present application just the inverse is true. The principal reason for this is that in [12] the plasma potential is assumed to be slightly positive which traps the (low energy) plasma electrons while in the EBGP-source the space charge potential is negative which lets the plasma electrons escape and traps the ions.

The magnitude of the difference between the anode and the plasma potential ($\Delta\phi$ in fig. 1c and d) can be calculated if it is assumed that the ion velocities follow a Maxwell distribution. For a one-dimensional "ion gas" of temperature T, and an ion of mass m the probability that the ion velocity u (in one direction) falls in the interval u, $u + du$ is $f(u)du$; with

$$f(u) = \left(\frac{m}{2\pi kT}\right)^{1/2} e^{-\frac{mu^2}{2kT}} \quad . \tag{16}$$

The ion current to the anode in this velocity interval then is:

$$dI_A = e\, n\, f(u)du \quad . \tag{17}$$

To overcome the space charge potential $\Delta\phi$ the velocity u has to meet the condition

$$\frac{m}{2} u^2 \geq e\Delta\phi \quad . \tag{18}$$

The lowest value of u which satisfies this condition is:

$$\check{u} = \left(\frac{2e\Delta\phi}{m}\right)^{1/2} \quad . \tag{19}$$

The total ion current which leaves the plasma then is:

$$I_A(\Delta\phi) = \int_{\check{u}}^{\infty} e\, n\, f(u) u\, du \quad . \tag{20}$$

Substituting eq. 16 and integrating yields:

$$I_A(\Delta\phi) = I_A^o\, e^{-\frac{e\Delta\phi}{kT}} \quad , \tag{21}$$

where I_A^o is $I_A(\Delta\phi = 0)$.

Eq. (21) can be rearranged as follows:

$$|\Delta\phi| = \frac{kT}{e} \ln \frac{I_A^o}{I_A} \quad , \tag{21a}$$

or $$|\Delta\phi| = 8.61 \times 10^{-5} T \ln \frac{I_A^o}{I_A} \ (V) \quad . \tag{21b}$$

If one imposes the arbitrary requirement that 99% of all singly charged ions at a temperature of 3000 K should be trapped, it follows from eq. (21b) that $|\Delta\phi| = 1.2$ V. This also shows that the primary electron energy is diminished only very slightly as the electrons enter the ionizing volume.

3.3 Space Charge Compensation

The concept of a space charge compensated electron bombardment source requires that the space charge generated by the primary electrons ρ_e is compensated by the ion space charge ρ_i:

$$\rho_e + \rho_i \approx 0 \quad . \tag{22}$$

Since space charge ρ, current density J and velocity v of the charge carrier are related via $\rho = J/v$ it follows that space charge compensation is achieved if

$$\frac{J_e}{J_i} = \frac{v_e}{v_i} \quad . \tag{23}$$

The mean thermal ion velocity <u>in one direction</u> is:

$$v_i = \sqrt{\frac{2kT}{\pi m_i}} \tag{24}$$

or $$v_i = 72.75 \sqrt{T_i/M_i} \quad \text{(m/s)} \quad . \tag{24a}$$

The electron velocity is

$$v_e = 6.73 \times 10^3 \sqrt{T_e} \quad \text{(m/s)} \quad . \tag{25}$$

Equations (23), (24a), and (25) combined give

$$\frac{J_e}{J_i} = 92.5 \sqrt{\frac{T_e}{T_i} M_i} \quad . \tag{26}$$

For $T_e = 1.2 \times 10^6$ K($\hat{=}$ 100 eV), $T_i = 3000$ K, $J_e = 5.5 \times 10^3$ A/m^2 (including a reflection factor of 1.4) and an average ion mass $M_i = 84$, eq. (26) yields $J_i = 5.9 \times 10^{-5}\ J_e = .32$ A/m^2. This is the ion current density near the anode grid. On the axis of the source the electron current density and therefore also the ion current density are higher by a factor κ. The magnitude of this factor is difficult to estimate, but computer studies show (c.f. section 6) that for the EBGP source κ is about 5, and the ion current density J_i^* near the extraction opening is therefore $J_i^* \approx \kappa\ J_i \approx 1.6$ A/m^2. It should be pointed out again that this is an <u>internal</u> ion current that does <u>not</u> reach the anode grid or the cathode; it is, however, the current density of the <u>extracted</u> beam measured at the extraction opening. Since the area of the exit opening is 1.8×10^{-6} m^2, the total extracted current is 2.9 μA which is the correct order of magnitude observed in experiments.

4. Experimental Results

Several experimental results were already reported in previous sections. In section 2. the operating principle of the new source was characterized as an electron-beam-generated plasma (EBGP). In a conventional plasma source the anode and cathode are immersed in the plasma with the characteristic formation of sheaths at the plasma/electrode interfaces. Several criteria exist for the stability of these sheaths and unless these criteria are fulfilled either a plasma can not be formed at all or the source behaviour is erratic. In practical terms this means that certain threshold values of the source parameters (gas pressure, electron current and temperature etc.) have to be reached before a plasma discharge can be initiated, at which point the values of several source parameters change abruptly. Such a behaviour is largely absent in an EBGP ion source. This can be seen from fig. 6 where the measured ionization efficiency η^* for trace amounts of Kr is plotted as a function of the electron bombardment current** for two electron energies $U_e = 100$ and 160 eV. A smooth behaviour of the Kr efficiency is observed for an electron current variation over two orders of magnitude, without any signs of instabilities. The fall of η(Kr) at higher electron currents is probably due to a higher residual gas pressure inside the ion source because of increased power dissipation. This is exemplified by the mass spectra shown in fig. 7b and c. In fig. 7c the electron bombardment and the total power into the source are 46 W and 380 W while for fig. 7b the values are 134 W and

---

*η is defined as the number of singly charged ions of a given species leaving the ion source per unit time divided by the number of neutral atoms entering the source per unit time (x 100%).

**The current variation was achieved by varying the cathode temperature.

440 W respectively. An 88 W increase in electron bombardment power (60 W in total power) raises the Ta and W currents by about two orders of magnitude. Even though some of this increase (at most a factor of 2) is due to enhanced ionization it clearly shows the elevated vapour pressures of the source materials.*

In general the EBGP source is not operated in the voltage (U_e) stabilized mode as shown in fig. 6 but in the current (I_e) stabilized mode depicted in fig. 8. It was found experimentally that the latter is more stable under the varying beam power conditions of the accelerator. (The power dissipated by the stopped, full energy heavy ion beam can amount to about 10% of the total ion source power and 25% of the electron bombardment power!)

To further elucidate the role of the background gas in the operation of the source an experiment was performed in which controlled amounts of argon gas were admitted to the ion source. The ionization efficiency $\eta(Kr)$ for trace amounts of Kr was measured as a function of the amount of argon in the source, as determined by the beam current at mass 40. The result is shown in fig. 9: $\eta(Kr)$ is essentially independent of the amount of argon present up to an Ar current of about 10 μA. Above this value the yield drops precipitously. In view of the operating model presented in section 2. this can be understood in the following way: up to certain pressure p^* ($\approx 2 \times 10^{-5}$ Torr for Ar) the ion production rate minus the loss due to extraction is lower than required to compensate the electron space charge, the space charge well remains negative, and all ions are trapped and eventually extracted: the source operates with high efficiency. At pressures above p^*

---

*To raise the vapour pressure of W by two orders of magnitude requires an increase of the "cold spot" temperature from about 2500 K to 2800 K.

the ion production rate becomes too high, the electron space charge gets overcompensated, the plasma-potential becomes positive, and ions start to flow towards the wall. These ions are lost for extraction and the source efficiency diminishes. The extracted current at which this happens can be calculated from equation (27) which relates the ion current density at the plasma boundary J_i to the ion density in the plasma n_i, the electron temperature T_e, and the ion mass number M_i [1]:

$$J_i = 1.45 \times 10^{-17}\ n_i\ \sqrt{T_e/M_i}\ \ (A/m^2) \quad . \tag{27}$$

In the case discussed above the ions will flow towards the wall as soon as $n_i \approx \nu n_e$. With $T_e = 1.2 \times 10^6$ K ($\approx$100 eV), $n_e = 4.1 \times 10^{15}\ m^{-3}$, $\nu = 1.4$ and $M_i = 40$ eq. (27) gives $J_i = 14\ A/m^2$; and since the area of the outlet opening is $1.8 \times 10^{-6}\ m^2$ the argon ion current limit is 25 μA which is in agreement with the experimental result shown in fig. 9.

It was calculated in section 3.2 that the negative plasma potential necessary to trap ions with thermal energies equivalent to 3000 K is about 1.2 V. This small potential is difficult to measure. An attempt was made to observe the change in plasma potential as Ar gas is admitted to the source while η(Kr) is being measured. The result of two independent experiments are shown in fig. 10 ($\Delta\phi^{(1)}$ and $\Delta\phi^{(2)}$). The change in plasma potential was deduced from the change in the position of the ^{86}Kr mass line in the focal plane of the separator magnet. At the same time the energy resolution R_E was determined from the ^{86}Kr peak width. At high ionization efficiencies (low Ar gas pressure) the plasma potential remains essentially constant independent of the Ar pressure. As the source efficiency diminishes the expected small increase in plasma potential is observed. For low η(Kr)

(high source pressure) ϕ drops sharply and the resolution <u>increases</u> by nearly a factor 3. Some of the latter effects are probably caused by a change in the shape of the plasma boundary at the extraction opening due to the high ion current density.

5. Mechnical and Electrical Aspects of the Source Design

The two most important parameters of an on-line isotope separator source are efficiency and speed. High efficiency of the EBGP-source has been achieved through the principle outlined in the previous sections. High speed on the other hand requires high temperature operation so that nuclear reaction recoils diffuse quickly out of the catcher material. A high operating temperature is also necessary to prevent the condensation of low vapour pressure materials on cold spots. The source shown schematically in fig. 11 has been built with these design goals in mind.

Nuclear reaction products enter the source from the left, traverse a bundle of capillary tubes and stop in the anode end plate which also acts as a catcher. The catcher is kept at a temperature just below 3000 K by internal electron bombardment heating from the cathode end plate and by the accelerator beam which also stops in the catcher. After diffusing out of the catcher the recoils are ionized in the anode volume and extracted through holes in the anode and cathode end plates as described previously. The ionization region is delimited by the anode grid which is surrounded by a closely spaced cathode. The cathode is heated by electron bombardment from a coaxial filament, which in turn is surrounded by several heat shields. The anode is kept 100 V positive, and the filament 2 KV negative with respect to the cathode. The source version shown in fig. 11 is intended for the study of compound nucleus reactions products that leave the target with a small angular divergence. For the study of other reactions the capillary tubes can be omitted and a window or target can be placed at the "target ring" location shown in fig. 11. By replacing the "anode grid" with a solid cylinder of Re, Ta, or W the source can be changed to a surface ionization

configuration (fig. 12). In this mode the anode volume is heated by electron bombardment from the cathode.

The purpose of the bundle of Ta capillary tubes is to let the highly directional recoils pass into the ionization region unhindered while keeping the thermalized recoils from diffusing back towards the colder parts of the ion source. The molecular flow conductance ratio R between a large tube of diameter D and the same tube filled with capillary tubes of diameter d is approximately $R \approx D/d$; d is chosen such that the conductance through the bundle of capillaries is small compared to the conductance of the hole in the anode.

Several other design details are of importance:

(1) To obtain the shortest possible diffusion times the operating temperature of the Ta catcher is kept close to 3000 K which is higher than the "cold spot" temperature of the source. At 3000 K .5 mm of Ta catcher material will evaporate in about 24 hrs.

(2) There are <u>no insulators</u> in the hot sections of the ion source. The source is kept tight through long narrow slots which act as molecular flow restrictions (typical spacing .25 mm). Outgassing from insulators would raise the background pressure above the critical level and destroy the high ionization efficiency as discussed in section 4.

(3) The coaxial construction of the source prevents uneven thermal expansion of the electrodes that would close off the small molecular flow gaps and cause electrical shorts. It also assures that the outer electrodes act as active heat shields for the inner parts.

(4) The volume of the ionization region is only .4 cm^3 which is the main reason for the observed short hold up time. (In on-line runs ^{155}Lu ($T_{1/2}$ = 70 ms) has been observed.)

(5) The source requires no magnetic field. The current to the electron bombardment filament is supplied in such a way that its magnetic field near the source axis is zero. A strong magnetic field would influence the radial motion of the ionizing electrons and interfere with the efficient operation of the source. The absence of a magnetic field is probably also responsible for the good ion beam quality since magnetic fields are often associated with plasma instabilities.

The electrical supplies connected to the ion source are shown in fig. 13. All important parameters are monitored by a computer, which also controls the electron emission of the filament which in turn controls the cathode temperature. The computer can be programmed to stabilize either the anode voltage (U_a), the anode current (I_a) or the anode power. The anode power supply can be operated in a constant current or constant voltage mode.

6. Computer Simulation

There is a fundammental difficulty in the theoretical treatment of an EBGP ion source in cylindrical geometry as shown in fig. 1. If it is assumed that (1) the anode grid is an ideal, infinitely thin, transparent cylinder located coaxially inside the cathode and that (2) the initial, tangential velocity component of the electrons is zero, all electrons will follow radial trajectories and converge on the cylinder axis. This in turn will give rise to infinitely high electron and ion densities, and therefore such a model clearly has little practical value. In the actual device the two assumptions are, however, not correct, in particular the discrete structure of the anode grid wires introduces distortions of the concentric electric field lines between the anode and cathode that significantly alter the electron trajectories. The magnitude of these distortions can not be calculated analytically and a computer simulation is the most expedient way to get a quantitative impression of this effect. The simulation was carried out with the SLAC Electron Trajectory Program (EGUN) written by W. B. Herrmannsfeldt. It computes trajectories of charged particles in electrostatic and magnetostatic focusing systems including the effects of space-charge and self-magnetic fields. The program solves Poisson's equation by finite difference equations using the appropriate boundary conditions. It starts out by first solving Laplace's equation ($\rho = 0$) followed by electron trajectory calculations (still with $\rho = 0$). Secondly the space charge distribution is calculated and used as input for the next iteration which solves Poisson's equation ($\rho \neq 0$). Several iterations of trajectory- and space charge-calculations followed by solving Poisson's equation are carried out until the solution has converged sufficiently. Emission limited as well as space charge limited cathodes can be specified and a perpendicular component to the

electron velocity due to the temperature of the cathode can be introduced. The total cathode current is divided equally among the specified number of rays (typically 200).

Figs. 14-17 show the results of some calculations. Common to all calculations is the geometry of the cathode and the anode grid, and the anode- and cathode potentials of 100 and 0 V respectively. Equipotential lines are drawn starting at 5 V (near the cathode) in 10 V steps up to 85 V and for some grid wires up to 95 V. In figs. 14, 15, and 16 the cathode current densities are 10^3, 2×10^3, and 4×10^3 A/m^2 respectively. The left sides (a) of figs. 14-16 show the ion source without space charge compensation and the resultant formation of virtual cathodes. On the right sides (b) of the figures the source is fully space charge compensated and the electron trajectories are unaffected by the presence of the other electrons.

The following observations regarding the results of the calculations (figs. 14-17) can be made:

(1) The space-charge-well anticipated in chapter 2. for the start-up phase of the source is clearly reproduced.

(2) The location of the virtual cathode changes with the current density as predicted. For current densities of 10^3, 2×10^3, and 4×10^3 A/m^2 the distance D of the virtual cathode from the anode for a <u>planar</u> diode according to eq. 9 is 2.1, 1.5, and 1.1 mm respectively. The computer simulations for the <u>cylindrical</u> case shown in figs. 14a-16a give values of 2.3, 1.1, and 0.6 mm for the three current densities.

(3) The potential distribution between the anode wires and the cathode has a strongly defocusing effect on the electron trajectories and prevents excessively high charge densities on the source axis. From

the trajectories it can be estimated that the electron density near the center of the source is about 5 times higher than near the grid. ($\kappa = 5$ is also the value used in chapter 3.3.)

(4) Another contribution to the divergence of the electron trajectories comes from the thermal emission process at the cathode where the electrons receive a tangential velocity component proportional to $\sqrt{2kT_c/m_e}$ (T_c is the cathode temperature). This effect is demonstrated in fig. 17 for a cathode temperature of 2400 K. At each of 20 spots on the cathode 5 rays are started. The conditions for the computer calculations are chosen such that the central ray is unaffected by the cathode temperature and carries no current; the two rays next to it carry 45% ea. (22.5 A/m^2) of the current density and have a tangential velocity component of $\sqrt{2kT_c/m_e}$, while the outermost rays carry 5% ea. (2.5 A/m^2) of the current density and have a tangential velocity component of $2\sqrt{2kT_c/m_e}$. (Each of the 20 spots on the cathode carries 1/20th of the total cathode current density; in this case $1/20 \times 10^3 = 50$ A/m^2.)
In the uncompensated case shown in fig. 17a two rays have sufficient energy to overcome the potential barrier of the virtual cathode. Comparing fig. 17b with fig. 14b for instance it is evident that the "thermal divergence" contributes significantly to the reduction of the charge carrier densities near the axis.

(5) In the compensated as well as in the uncompensated case many electrons can be seen to "orbit" the anode wires which contributes to their ionization path length.

(6) A final remark concerning the computer simulation itself: Despite a considerable effort the calculations show slight imperfections.

These are mostly due to (a) the finite number of grid points, (b) the limited number of rays (this is particuarly evident in fig. 17a), (c) the finite accuracy in the ray tracing routine, and (d) the fact that the calculations were carried out only for the upper half of each picture which was then combined with its mirror image to compose the entire figure.

7. Conclusion and Acknowledgments

The ion source described in this communication has been used in several on-line and off-line experiments at the OASIS facility. It shows many of the desirable characteristics of an ideal on-line source, among them high speed and efficiency. The high efficiency is due to an electron-beam-generated plasma that traps ions and permits their efficient extraction, and the high speed is related to the small source dimensions and the high operating temperatures. The source incorporates no magnetic fields and is very stable. It requires no support gas per se and delivers beams of high quality witnessed by the high mass resolution that is obtained in conjunction with the mass spectrometer. The application of this source is not limited to on-line isotope separation purposes. Due to its high efficiency and high temperature operation it is ideally suited for the tracer ionization of all materials up to the highest melting points. Its low current output is advantageous for isotope separators with electrostatic focusing and deflection elements that are not space charge compensated.

It is a pleasure to thank several co-workers and colleagues for their help in the development of this source, in particular L. Archambault who performed all of the precision mechanical work. W. Kunkel and H. Kim helped in the understanding of the operating principle through several fruitful discussions. A. Wydler built the electrical supplies and the computer interfaces and R. Leres helped with the software. W. B. Herrmannsfeldt made his SLAC EGUN program available to us and helped to get it running on the VAX computers at LBL. R. Babala and P.Lemmertz adapted the program to the special geometry of the EBGP ion source and carried out many calculations including those shown in Figs. 14-17.

This work was supported by the Director, Office of Energy Research, Division of Nuclear Physics of the Office of High Energy and Nuclear Physics of the U.S. Department of Energy under Contract No. DE-AC03-76SF00098.

8. References

[1] A. Guthrie and R. V. Wakerling, eds., "The Characterisictics of Electrical Discharges in Magnetic Fields" (New York, 1949).

[2] R. Kirchner, K. H. Burkard, W. Hüller and O. Klepper, Nucl. Instr. and Meth. 186 (1981) 295.

[3] R. Kirchner, ibid. p. 275.

[4] G. Sidenius, Radiation Effects 44 (1979) 145.

[5] J. M. Nitschke, Nucl. Instr. and Meth. 206 (1983) 341.

[6] K. H. Kingdon, Phys. Rev. 21 (1923) 408.

[7] D. Rapp and P. Englander-Golden, J. Chem. Phys. 43 (1965) 1464.

[8] L. J. Kieffer and G. H. Dunn, Rev. Mod. Phys. 38 (1966) 1.

[9] M. v. Ardenne, "Tabellen zur angewandten Physik," Band I (1979) 592.

[10] M. Mitchner and C. H. Kruger Jr., "Partially Ionized Gases" (John Wiley & Sons, New York, 1973) p. 104.

[11] ibid. p. 109.

[12] D. A. Dunn and S. A. Self, J. Appl. Phys. 35 (1964) 113.

Figure captions:

Fig. 1. Schematic representation of the electron-beam-generated plasma (EPGP) ion source. (a) Radial cut. (b) Axial cut: I_e = electron bombardment current, I_{ep} = plasma electron current, I_i = ion current, I_i^{ex} = extracted ion current, V_o = electron bombardment potential, V_{ex} = extraction potential. (c) Radial dependence of the potential V_e and the associated electron kinetic energy eU_e with space charge compensation (full line) and without space charge compensation (dotted line). D indicates the location of the virtual cathode in the absence of space charge compensation. $\Delta\phi$ = potential difference between plasma and anode. (d) Axial dependence of the plasma potential ϕ_p.

Fig. 2. (a) Planar diode to illustrate the concept of a "virtual cathode." V_o = electron accelerating potential, I_e = electron current.
(b) Potential $U_e = V_o + \phi$ (electron kinetic energy eU_e) as a function of the distance x from the anode. D is the location of the virtual cathode.

Fig. 3. Calculation of the electron kinetic energy $eU_e(x) = e(V_o + \phi_e(x))$ according to eq. (9a) for a cathode potential $V_o = 100$ V and three different current densities J_e. The anode is located at $x = 0$ (cf. fig. 2b). The locations of the virtual cathode D are indicated by arrows.

Fig. 4. Mass spectrum of the EBGP ion source with attached, calibrated leaks of $^{natl.}Ar$, $^{natl.}Kr$, and $^{natl.}Xe$. The spectrum was recorded with a Faraday cup in the focal plane of the OASIS isotope separator. A bias current of 10^{-12} A was used for the logarithmic electrometer. The operating conditions for the ion source were: $U_e = 170$ V, $I_e = 1.0$ A.

Fig. 5. Calculated relationship between the degree of ionization X, and the product of the differential ionization q_i and the average time $\bar{\tau}$ an atom spends inside the ionization volume. ^{20}Ne, ^{84}Kr, and ^{200}Hg are shown as examples. The experimentally observed degrees of ionization are about 60% of the calculated values. The calculation was carried out for an electron bombardment beam current density $J_e = 3.9 \times 10^3$ A/m^2 and a reflection factor $\nu = 1.4$.

Fig. 6. Measured krypton ionization efficiency $\eta(Kr)$ of the EBGP ion source, as a function of the electron bombardment current I_e for two electron energies. (The highest $\eta(Kr)$ observed for a well out-gased ion source is 40%.)

Fig. 7. Portions of mass spectra recorded in the focal plane of the OASIS isotope separator with the EBGP ion source operated at two different power levels. (a) and (b): $I_e = 0.30$ A, $U_e = 153$ V, ($N_e = 46$ W), $N_{tot} =$ 380 W. (c): $I_e = 0.92$ A, $U_e = 146$ V, ($N_e = 134$ W), $N_{tot} = 440$ W.

Fig. 8. Measured krypton ionization efficiency $\eta(Kr)$ of the EBGP ion source, as a function of the electron bombardment potential U_e (electron energy eU_e). The electron current (I_e^{opt}) at each energy was optimized by varying the cathode temperature (emission limited mode). The optimum operating point for maximal $\eta(Kr)$ is $U_e = 170$ V and $I_e = .9$ A.

Fig. 9. The krypton tracer ionization efficiency $\eta(Kr)$, as a function of argon "background." (The Kr-current at $\eta(Kr) = 40\%$ is 5×10^{-8} A.) The argon background was measured as ion current at mass 40; it was varied by admitting Ar gas to the source through a variable leak valve.

Fig. 10. Change in plasma potential $\Delta\phi$ and energy resolution R_E as a function of $\eta(Kr)$, the tracer ionization efficiency for Kr. $\eta(Kr)$ was changed by admitting variable amounts of Ar to the source. The results of two different experiments are shown as $\Delta\phi^{(1)}$ and $\Delta\phi^{(2)}$.

Fig. 11. Schematic diagram of the EBGP-ion source as used in the OASIS facility. The version shown is intended for the study of compound nucleus reactions.

Fig. 12. Central parts of ion source (from left to right): a new surface ionization anode, a used EBGP anode, and a used cathode suited for either one of the anodes. Materials are tantalum and tungsten.

Fig. 13. Electrical connections to the ion source. The abbreviated parameters (I_{ex}, U_{eb}, U_e etc.) are monitored by a PDP 11/10 computer, which also controls the electron emission of the electron bombardment filament via the variable transformer.

Fig. 14. (a) Computer simulation of the EBGP source without space charge compensation. The potential between the cathode and the anode wires is 100 V. Equipotential lines are drawn starting at 5 V (near the cathode) in steps of 10 V up to 85 V. (Two grid wires show a 95 V potential line.) Inside the anode wire "cage" the space charge build up is quantitatively represented by equipotential lines of 85 V (95 V) near the anode wires descending in 10 V steps to 5 V towards the axis of the source. The virtual cathode is located 2.3 mm from the anode. The cathode current density of 10^3 A/m^2 is distributed among 194 rays. 96 rays are intercepted by the anode wire which is equivalent to a transmission of the anode grid of 50%. (b) The same conditions as (a) with space charge compensation. (Equipotential lines have been omitted.)

Fig. 15. Same conditions as in fig. 4 except that the cathode current density has been increased to 2×10^3 A/m^2. The virtual cathode (a) is located 1.1 mm from the anode.

Fig. 16. Same conditions as in fig. 14 except that the cathode current density has been increased to 4×10^3 A/m^2. The virtual cathode (a) is located .6 mm from the anode. Equipotential lines have been drawn (b) at 5, 15, 25, 35, 45, 55, 65, 75, and 85 V.

Fig. 17. Computer simulation of the EBGP source to show the influence of the cathode temperature on the electron trajectories. The anode-cathode potential and the total cathode current density are the same as in fig. 14. The cathode temperature is 2400 K. See text for details.

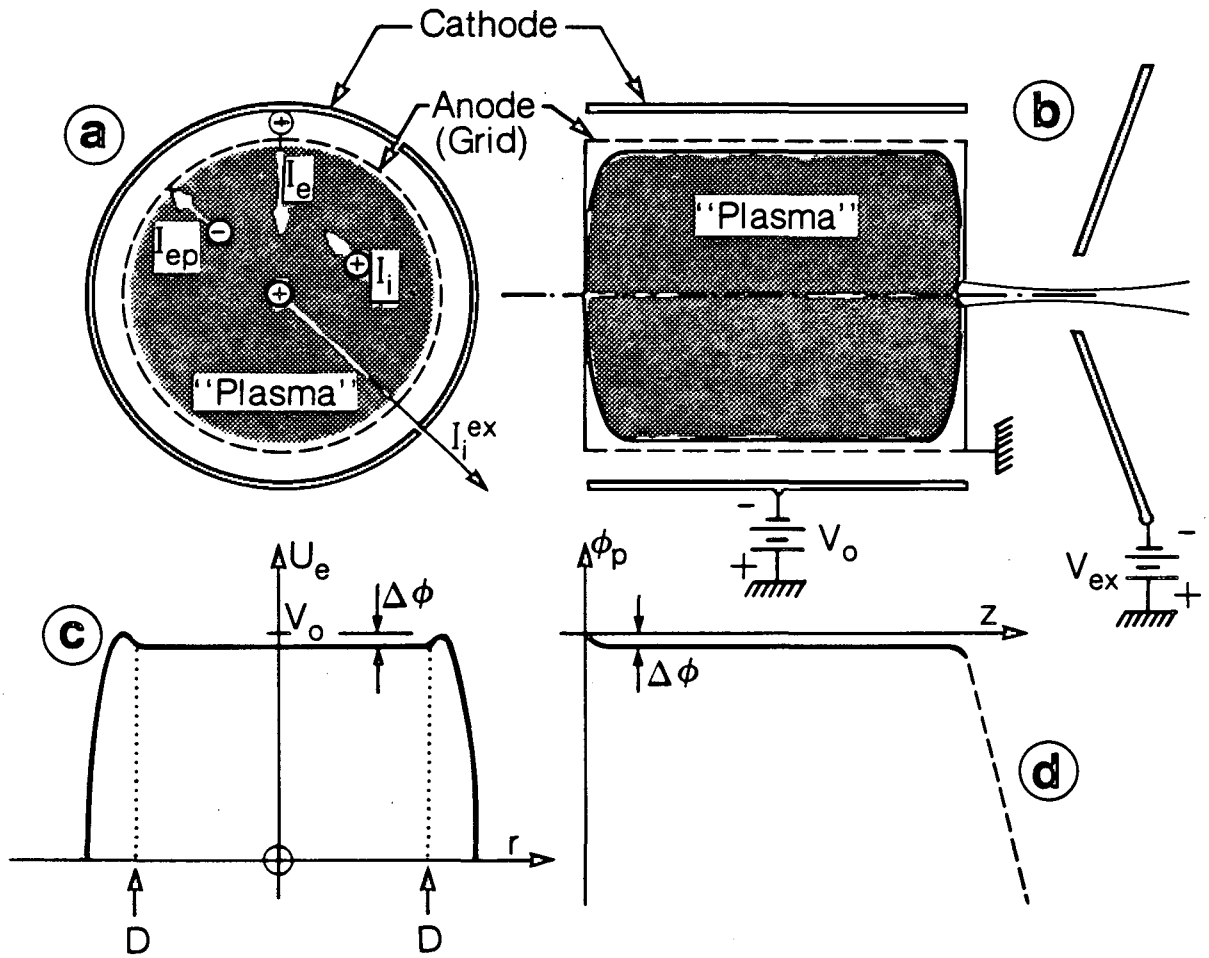

XBL 841-9458

Fig. 1

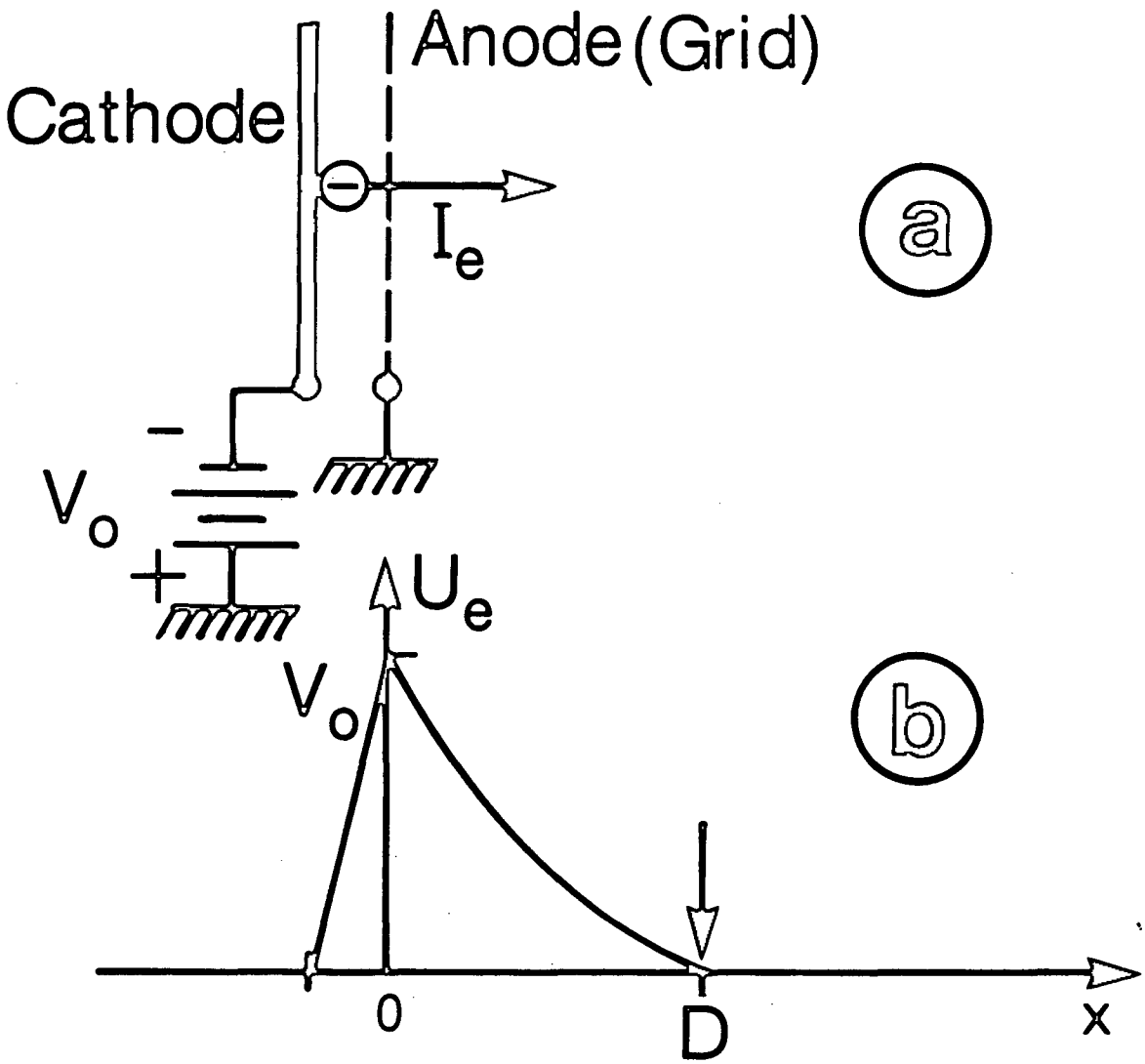

Fig. 2

XBL 841-9459

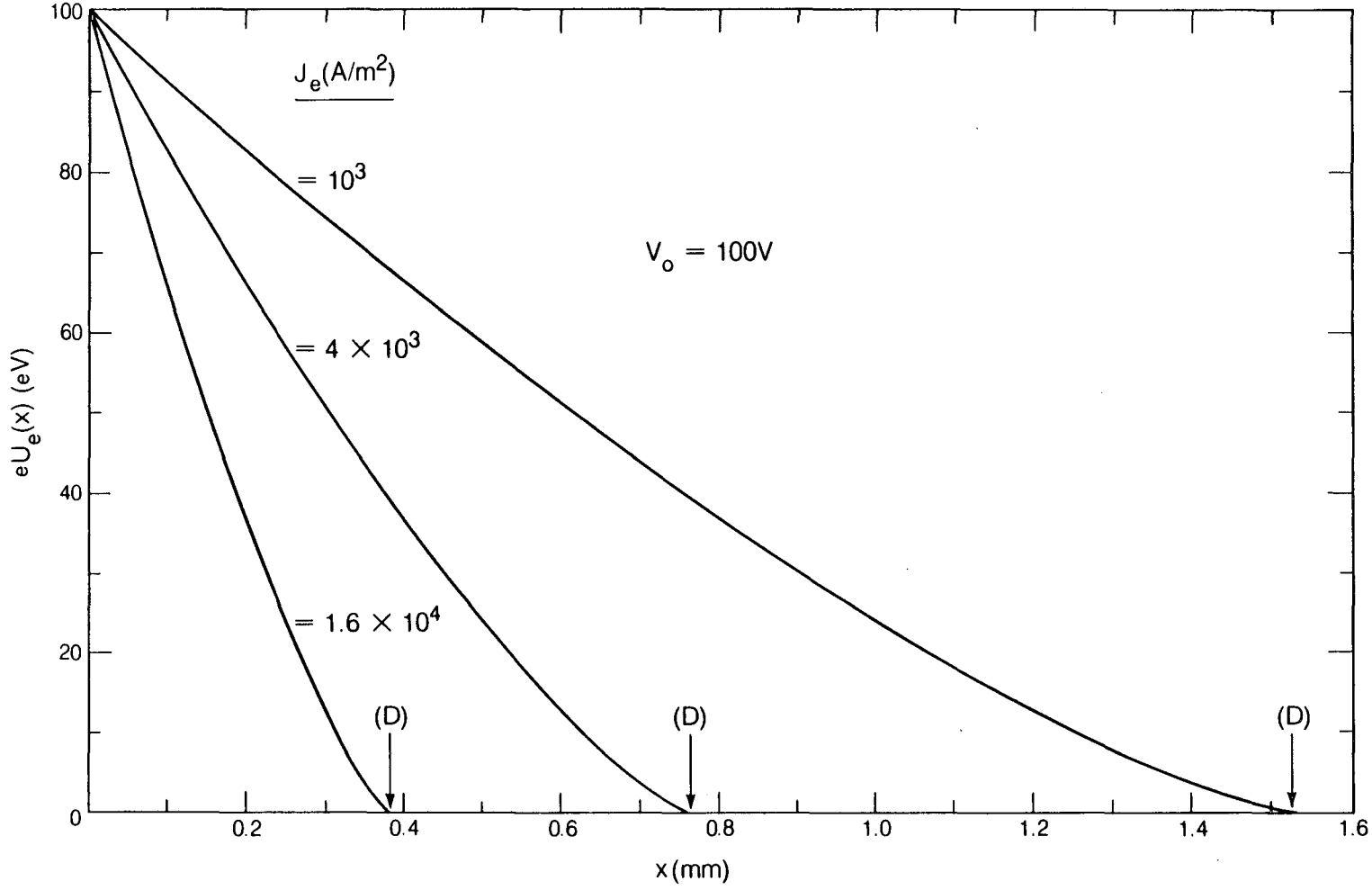

XBL 841-9467

Fig. 3

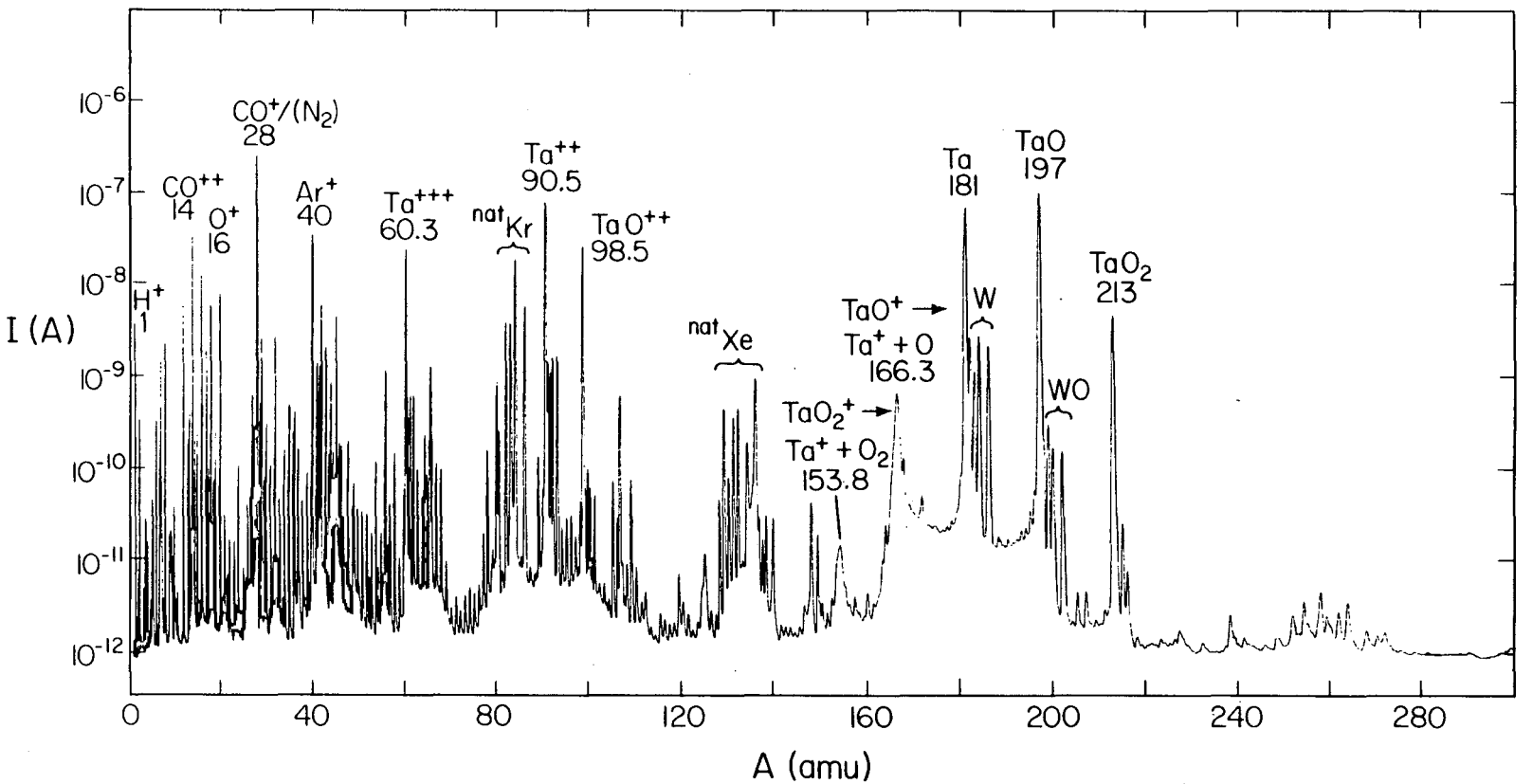

Fig. 4

XBL 827 – 974

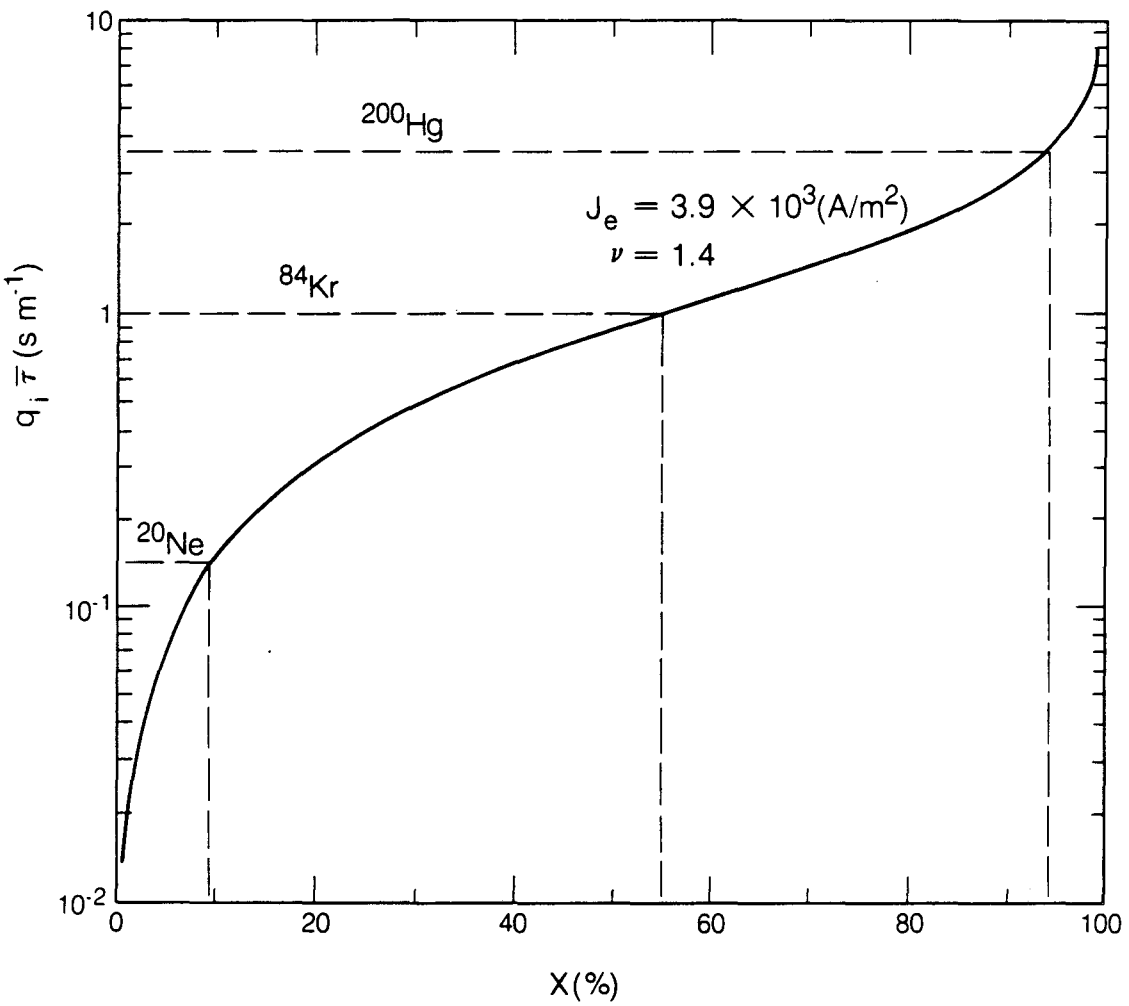

XBL 841-9464

Fig. 5

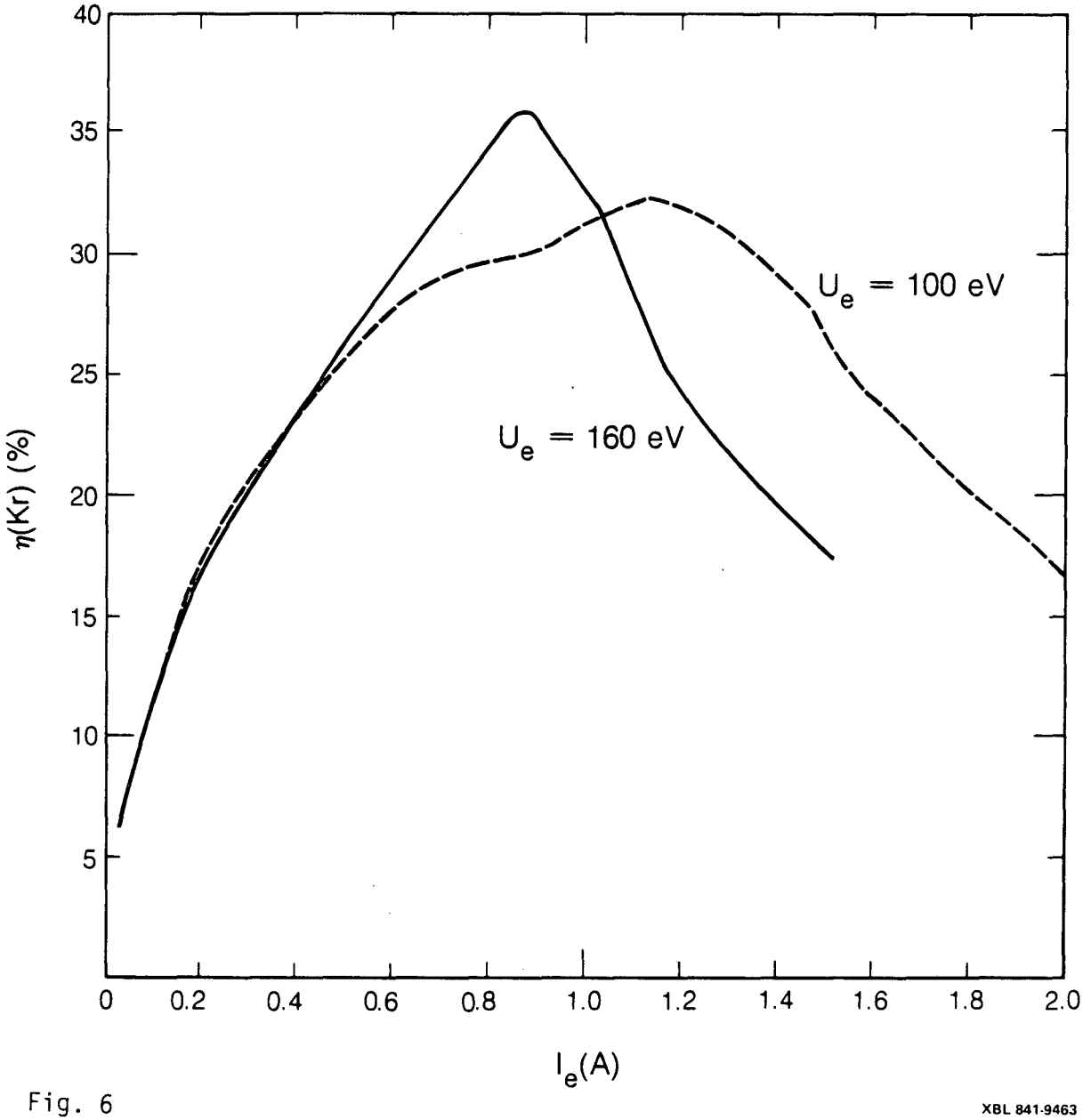

Fig. 6

XBL 841-9463

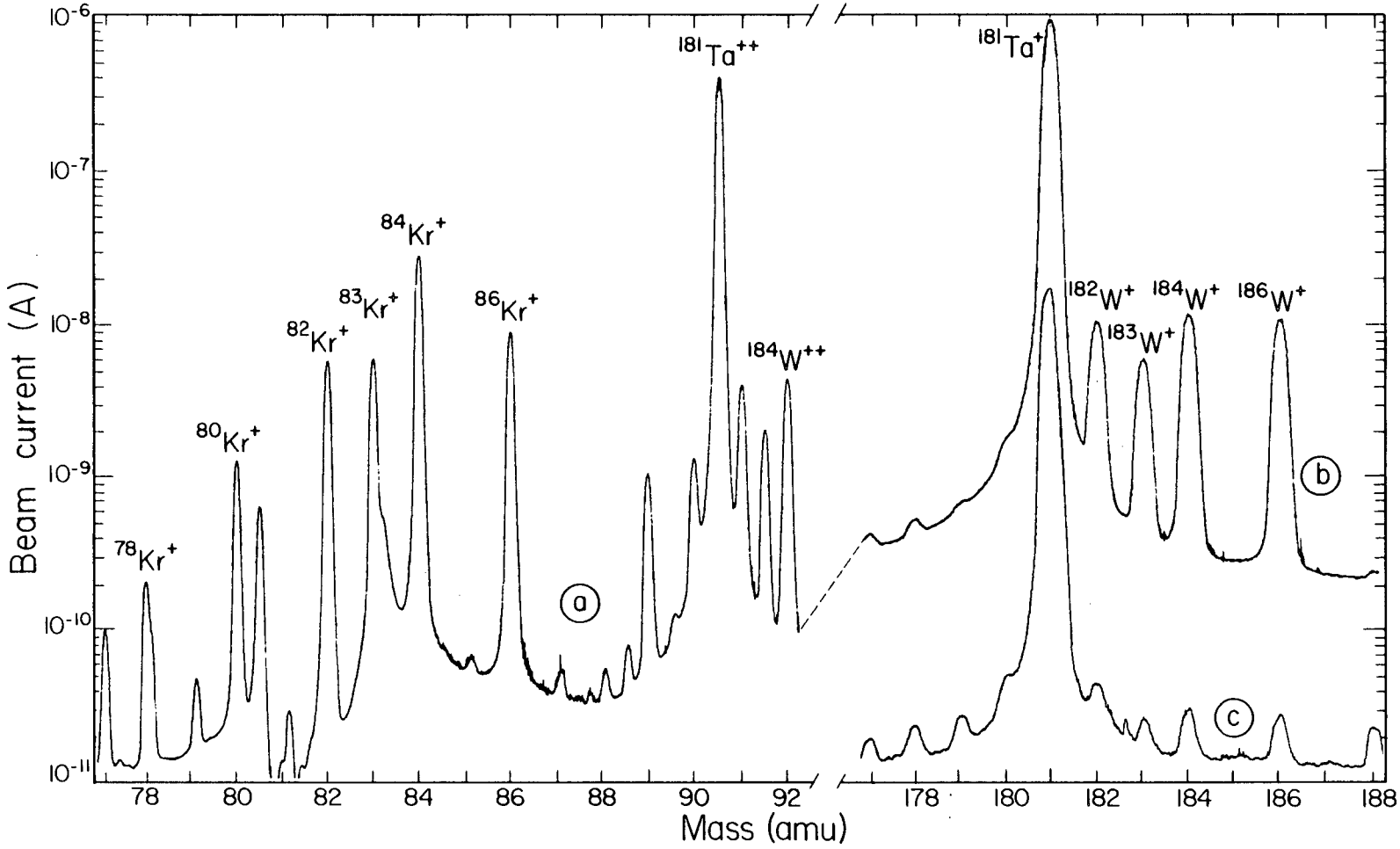

Fig. 7

XBL 827 – 973

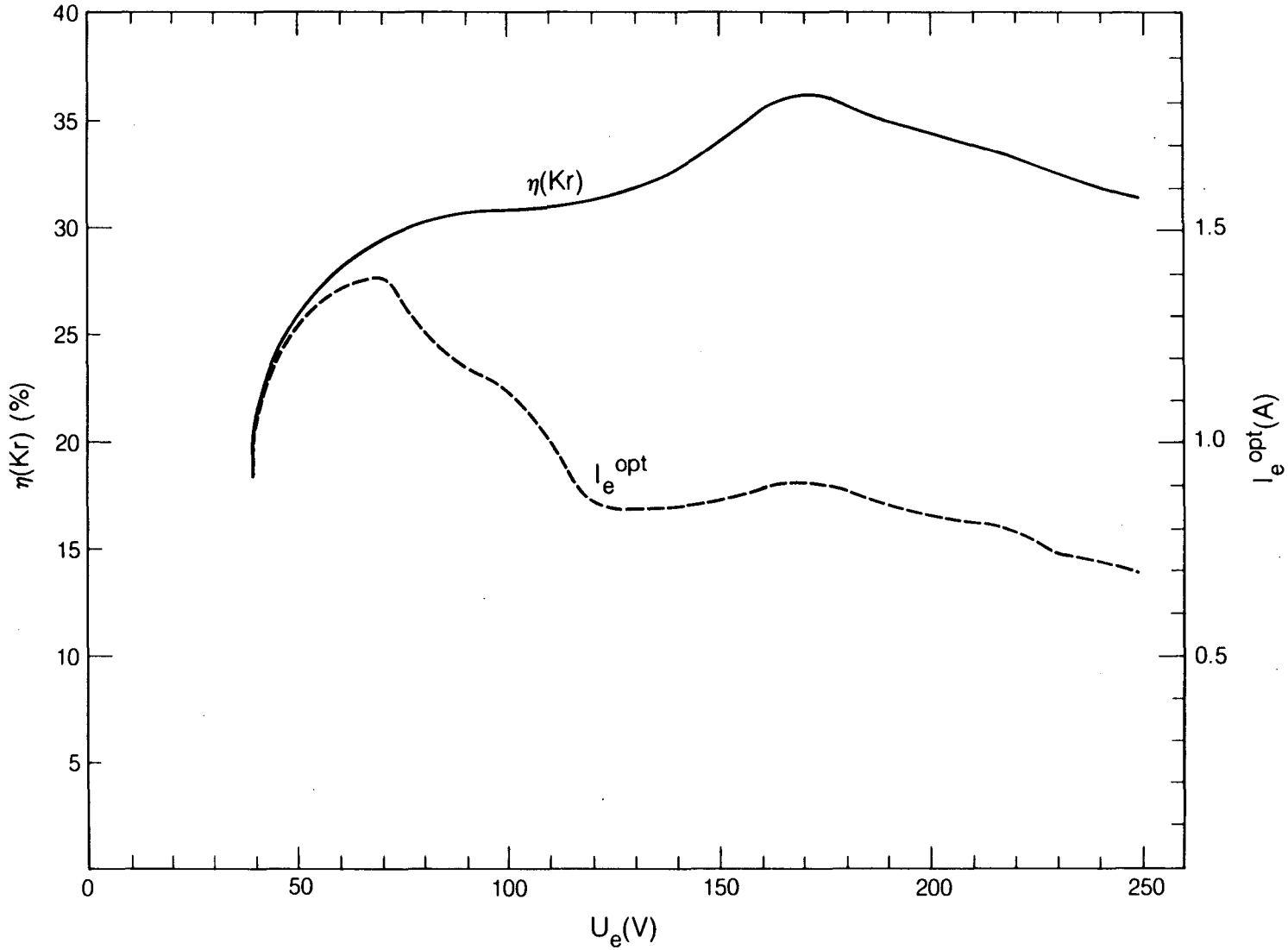

Fig. 8

XBL 841-9465

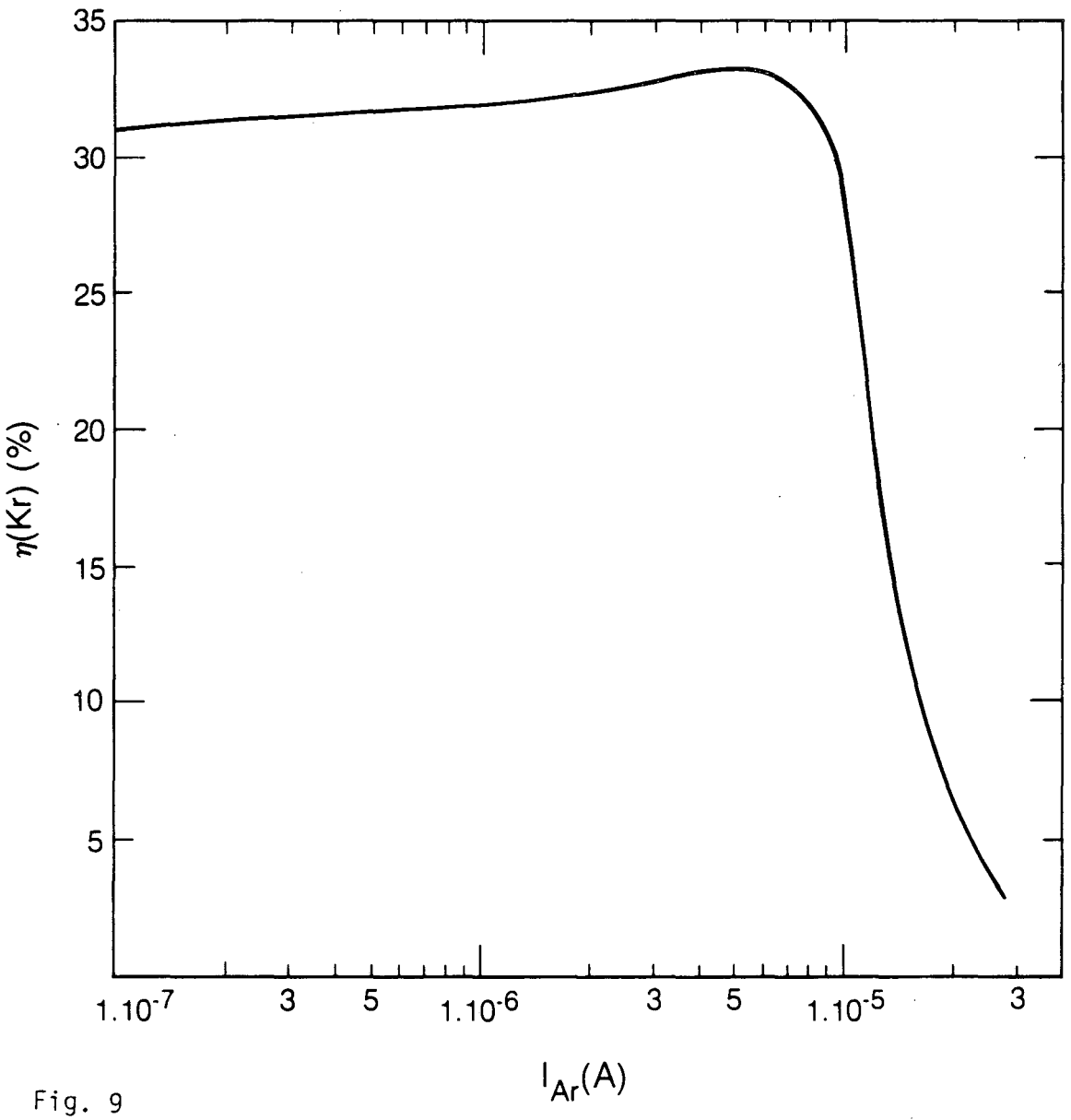

Fig. 9

XBL 841-9466

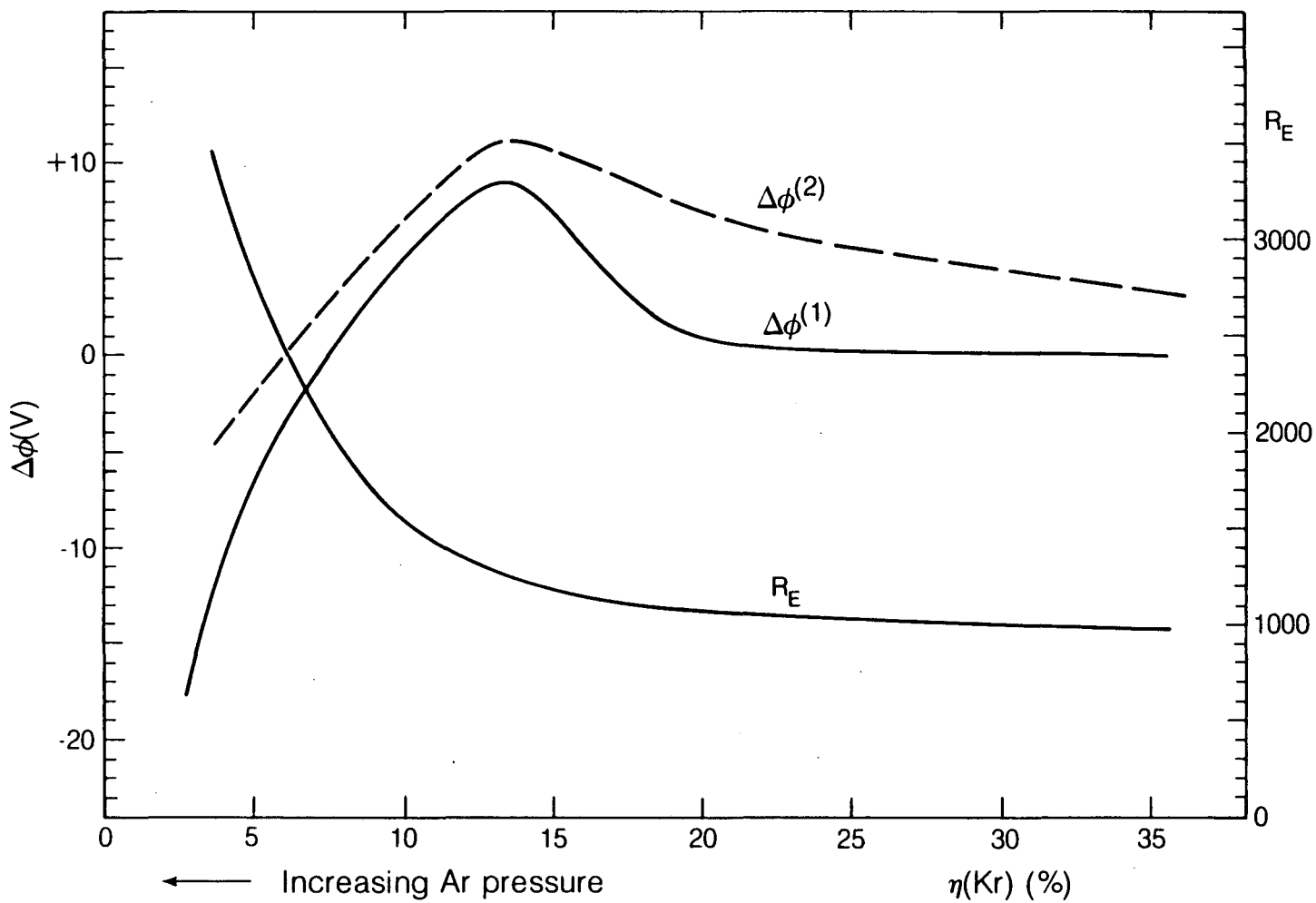

Fig. 10

XBL 841-9462

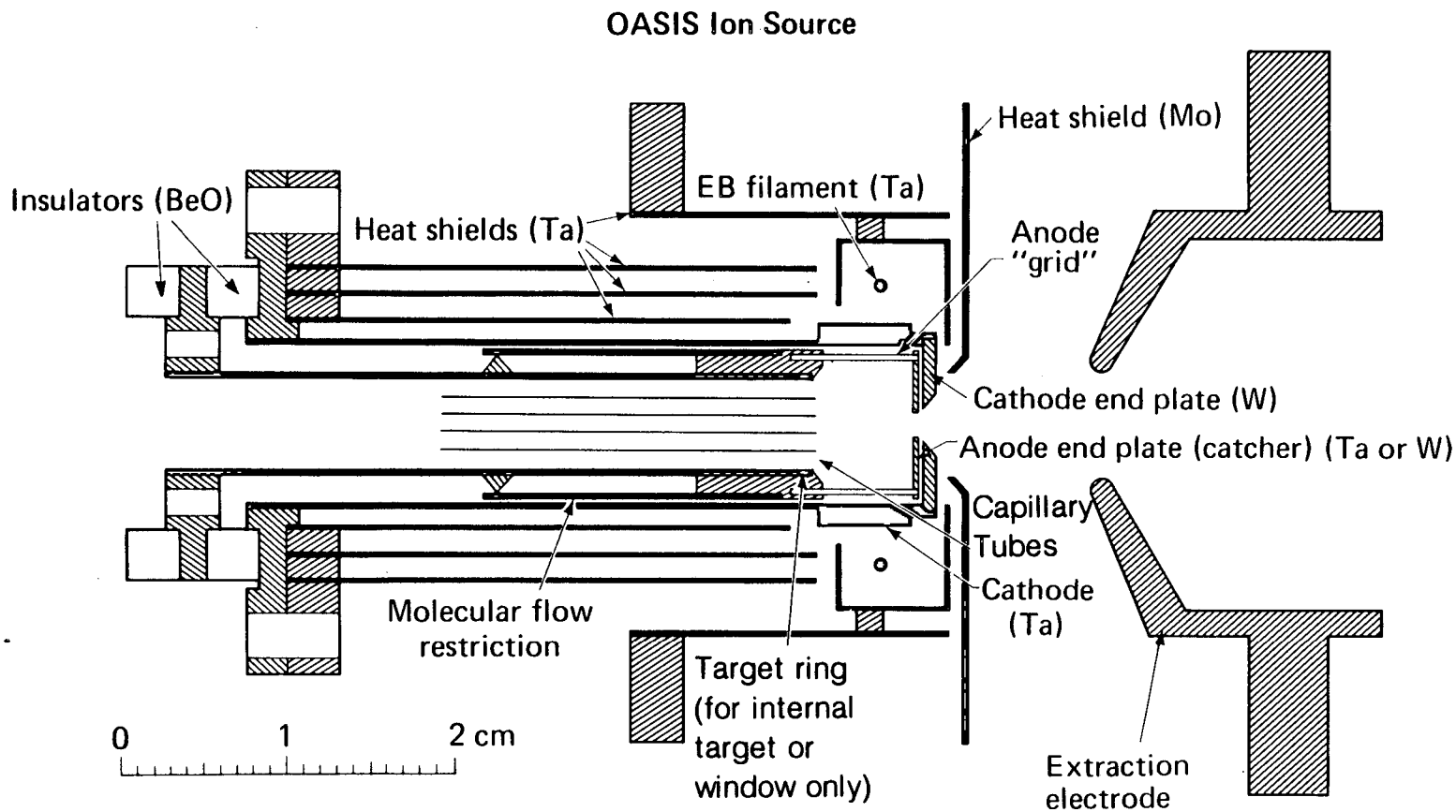

XBL 841-9460

Fig. 11

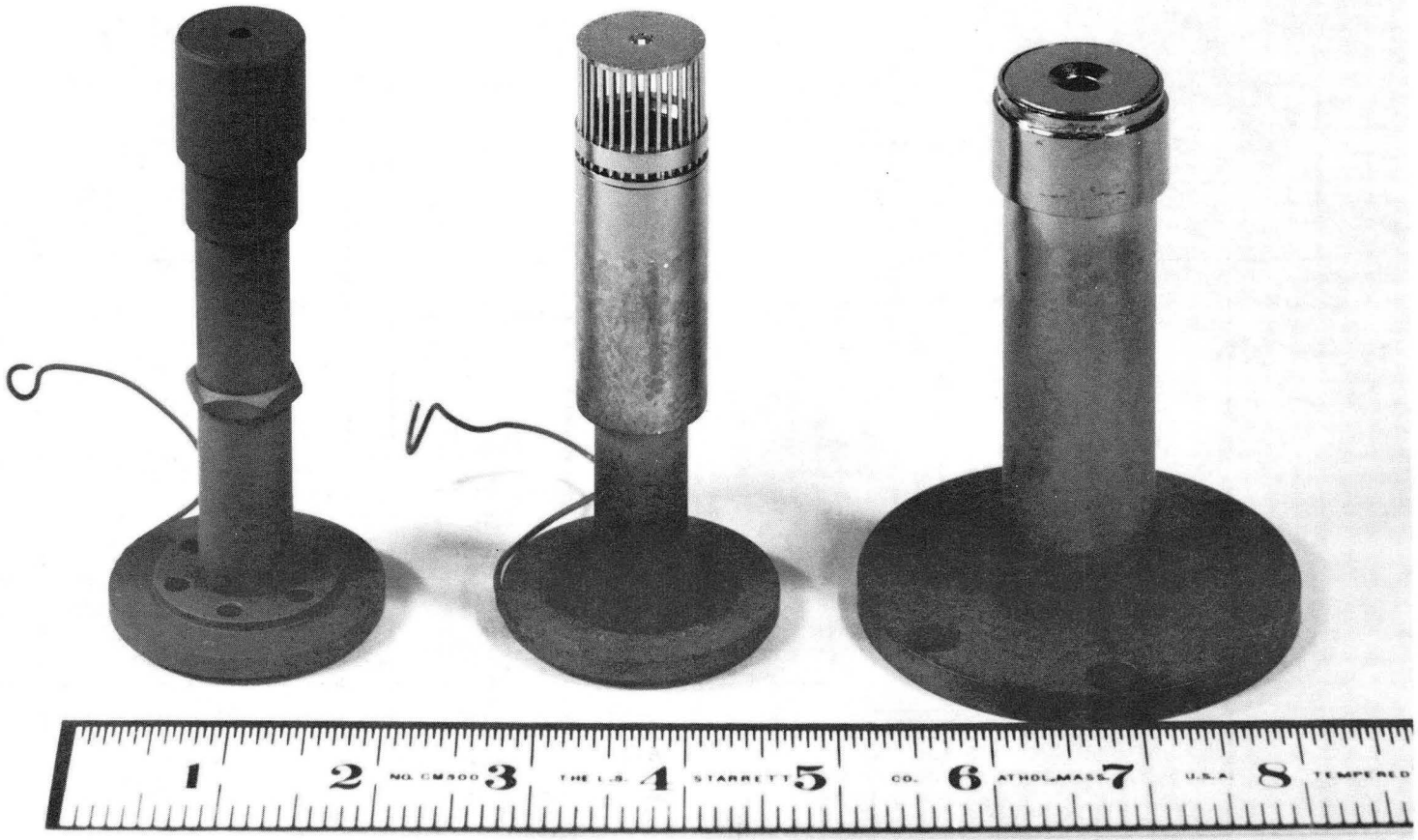

Fig. 1

CBB 823-2606

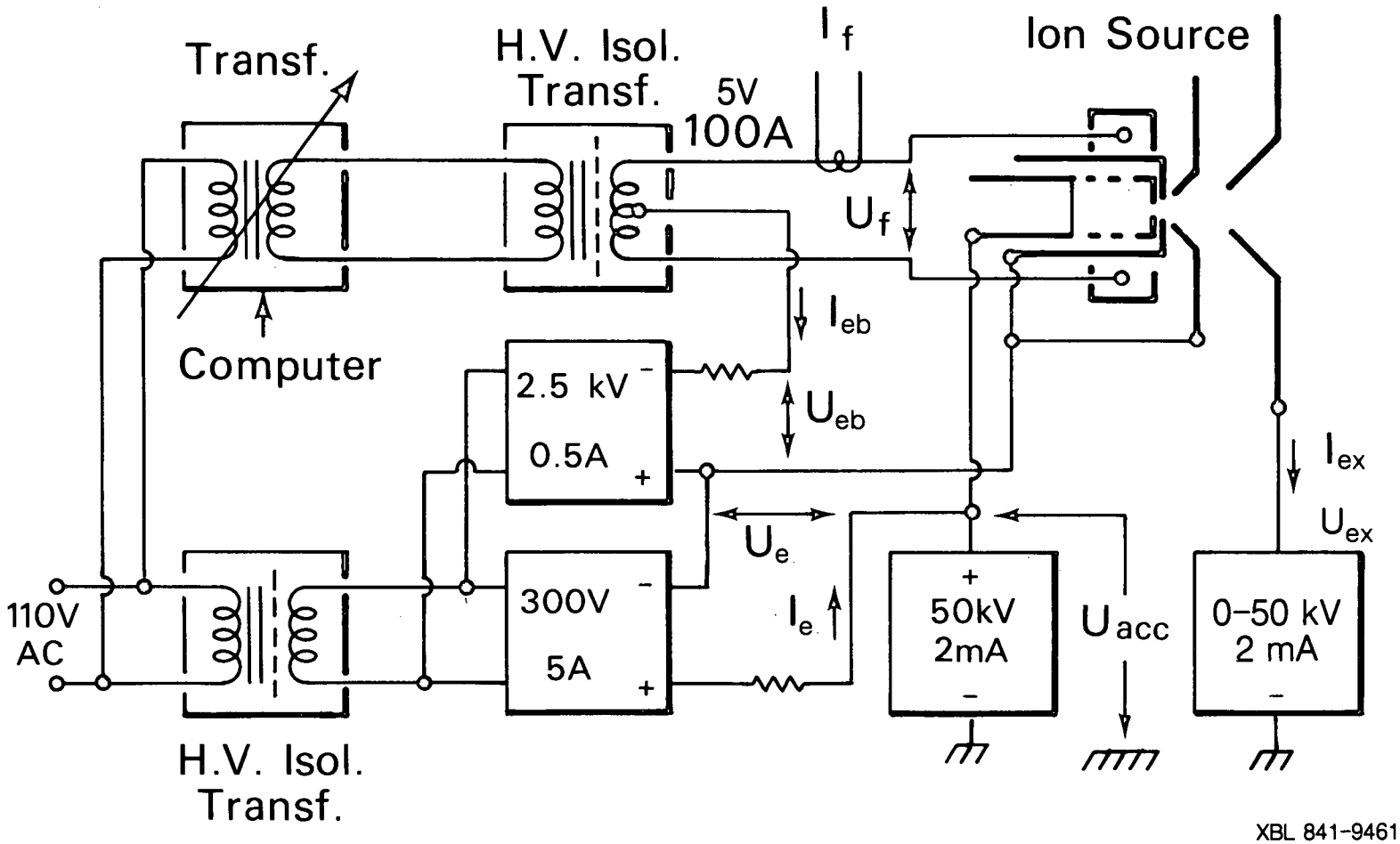
Transf.
H.V. Isol.
Transf.
5V
100A
I_f
Ion Source
U_f
I_{eb}
Computer
2.5 kV
0.5A
U_{eb}
I_{ex}
U_{ex}
U_e
110V
AC
300V
5A
I_e
50kV
2mA
U_{acc}
0-50 kV
2 mA
H.V. Isol.
Transf.
XBL 841-9461

Fig. 13

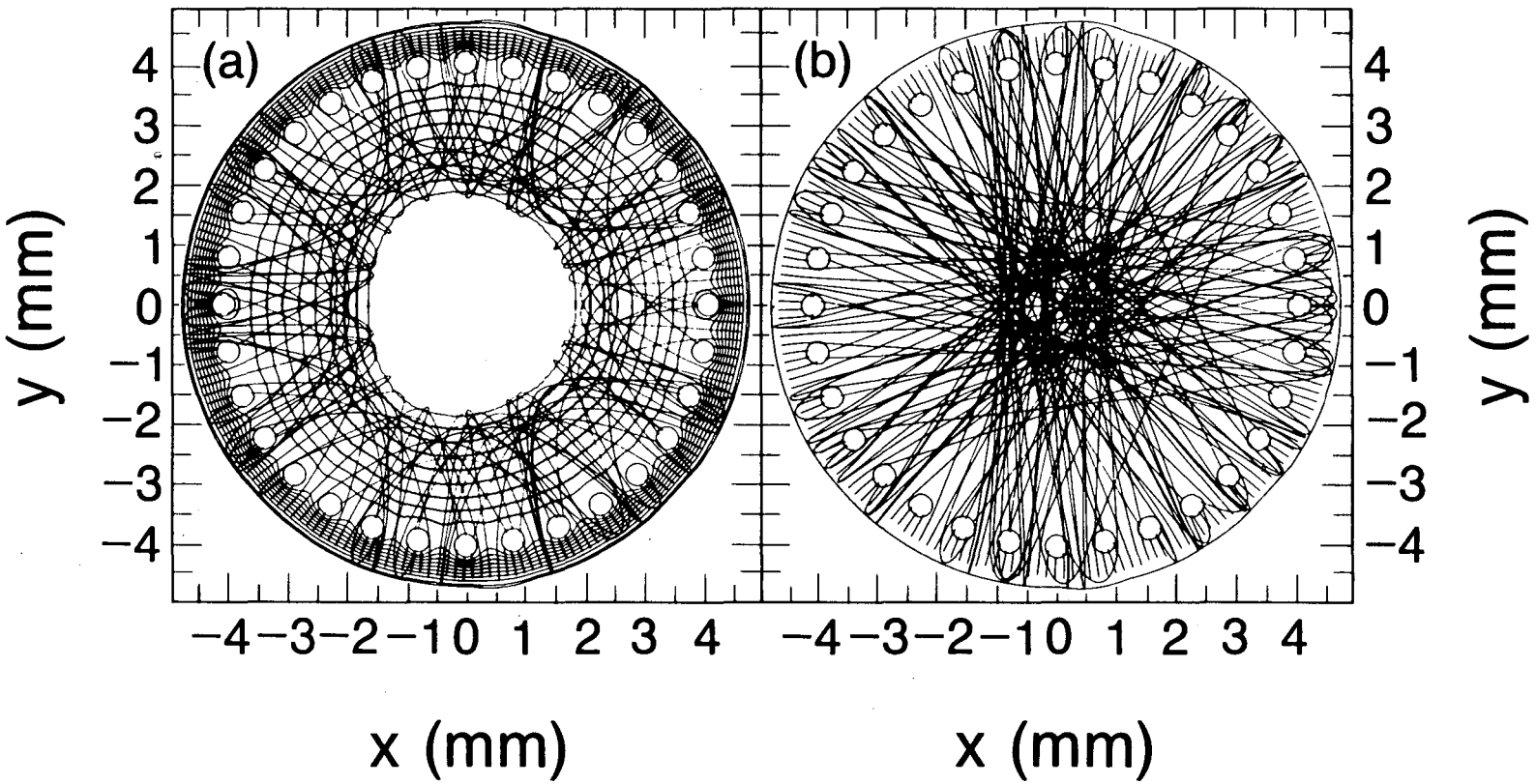

XBL 849-10769

Fig. 14

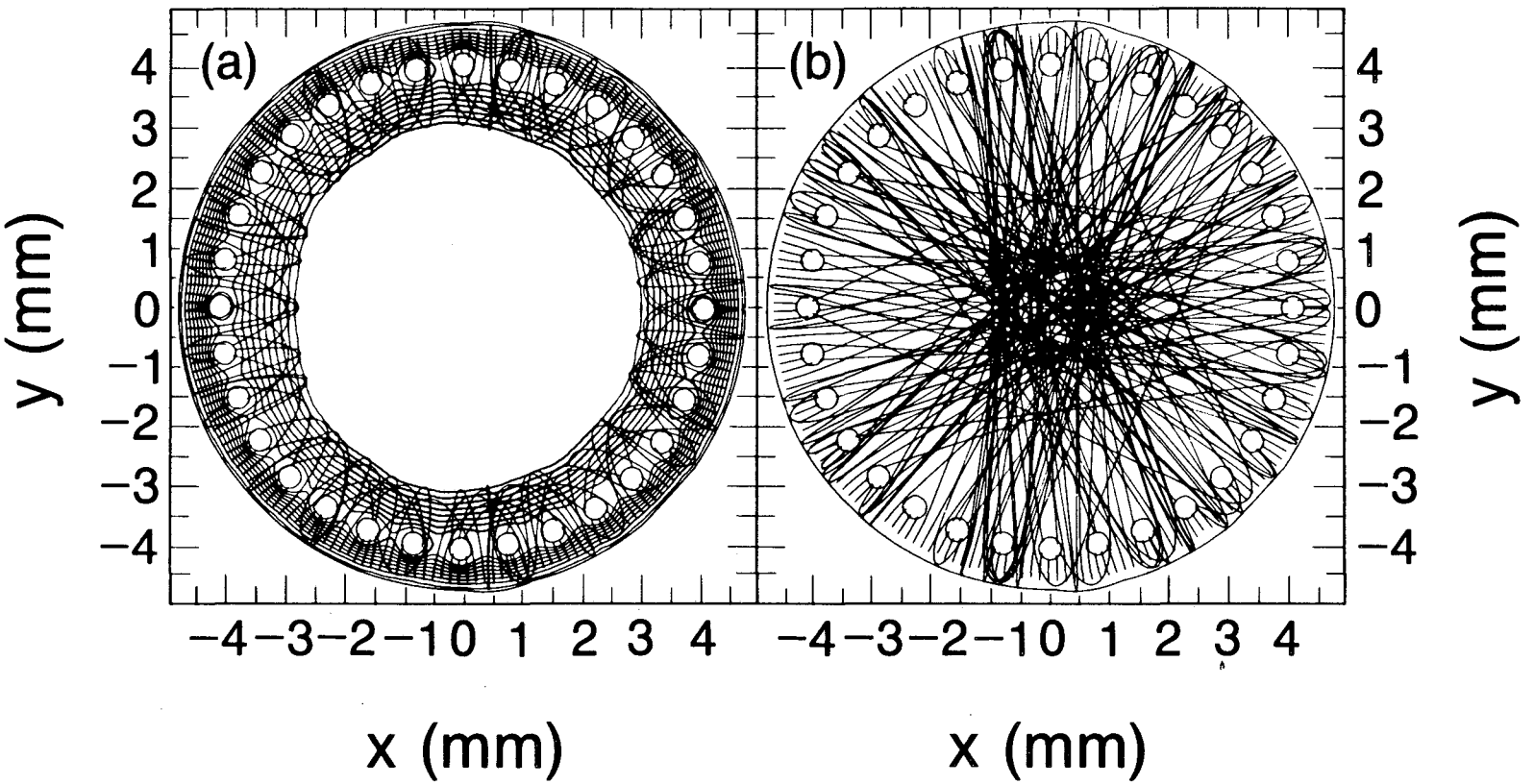

XBL 849-10770

Fig. 15

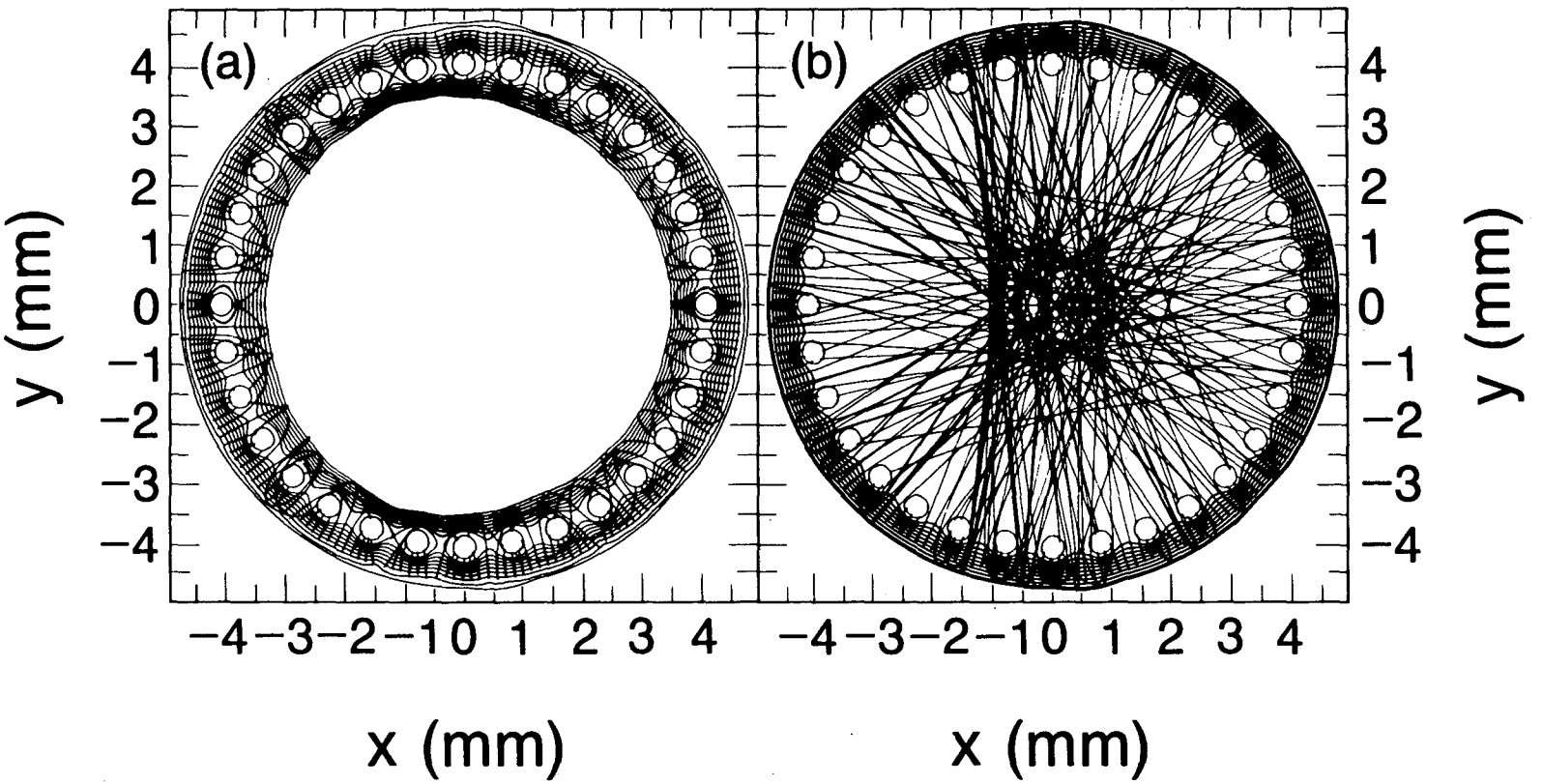

XBL 849-10772

Fig. 16

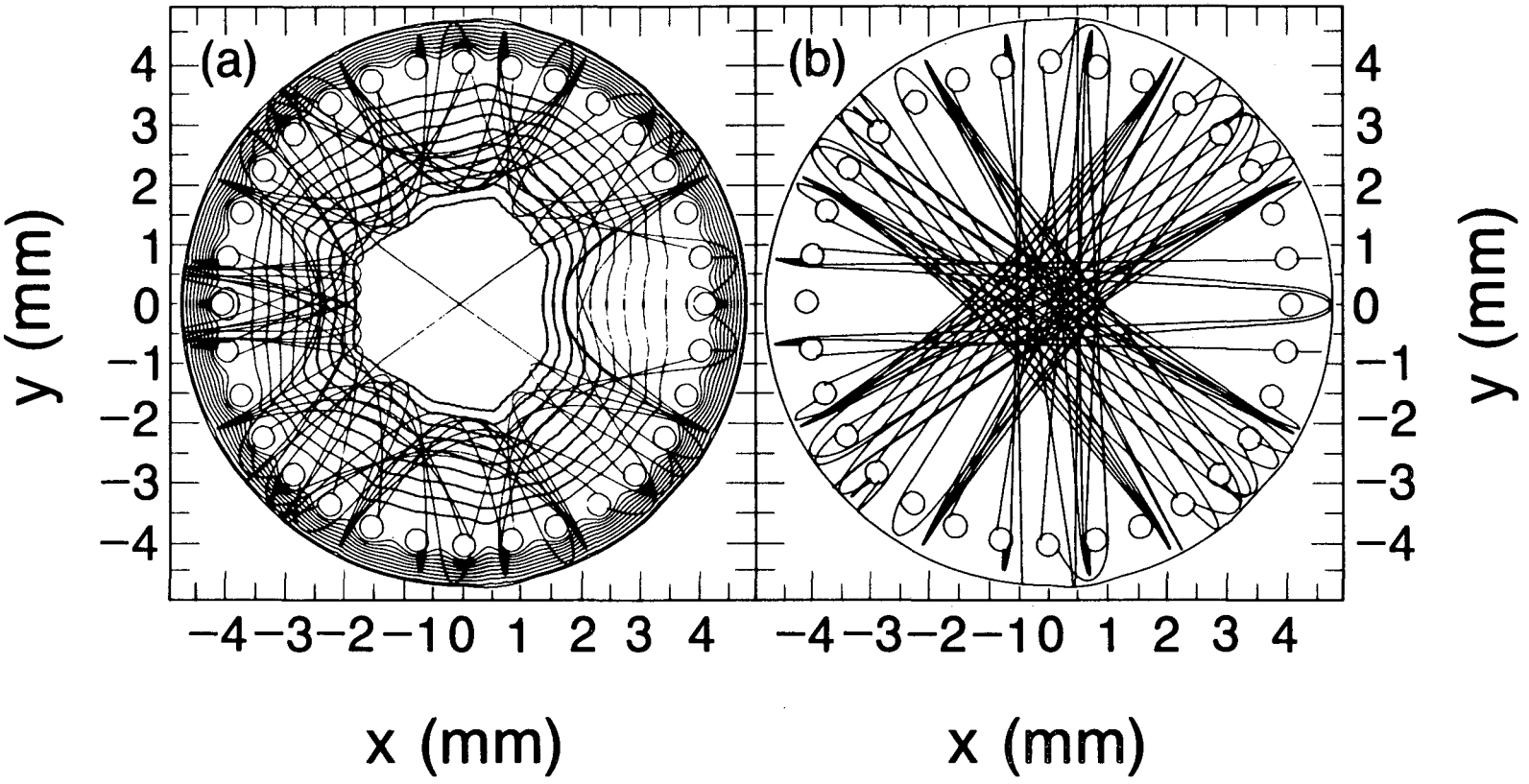

Fig. 17

XBL 849-10771

This report was done with support from the Department of Energy. Any conclusions or opinions expressed in this report represent solely those of the author(s) and not necessarily those of The Regents of the University of California, the Lawrence Berkeley Laboratory or the Department of Energy.

Reference to a company or product name does not imply approval or recommendation of the product by the University of California or the U.S. Department of Energy to the exclusion of others that may be suitable.

TECHNICAL INFORMATION DEPARTMENT
LAWRENCE BERKELEY LABORATORY
UNIVERSITY OF CALIFORNIA
BERKELEY, CALIFORNIA 94720